Human pluripotent stem cell-derived respiratory airway progenitors generate alveolar epithelial cells and recapitulate features of idiopathic pulmonary fibrosis

Mikael G. Pezet,[1]* Juan A. Torres,[1]* Tania A. Thimraj,[1] Ivana Matkovic Leko,[1] Nadine Schrode,[2,3] John W. Murray,[1] Kristin G. Beaumont,[2,3] Hans-Willem Snoeck.[1,4,5]

[1]Columbia Center for Stem Cell Therapies, Department of Medicine, Columbia University Vagelos College of Physicians and Surgeons, New York, NY, USA

[2]Department of Genetic and Genomic Sciences, Icahn School of Medicine at Mount Sinai, New York, USA

[3]The Center for Advanced Genomic Technology, Icahn School of Medicine at Mount Sinai, New York, USA

[4]Department of Microbiology and Immunology, Columbia University Vagelos College of Physicians and Surgeons, New York, NY, USA

[5]Division of Pulmonary Medicine, Allergy and Critical Care, Department of Medicine, Columbia University Irving Medical Center, New York, NY, USA

* Contributed equally to this work

Corresponding author:

Hans-Willem Snoeck, MD, PhD
Division of Pulmonary Medicine, Allergy and Critical Care
Columbia Center for Stem Cell Therapies
Departments of Medicine, and Microbiology & Immunology
Columbia University Vagelos College of Physicians and Surgeons
650 W. 168th Street, BB 801E
New York, NY 10032
(T) 212 342 0182
(F) 212 342 0550
email: hs2680@columbia.edu

Human lungs contain unique cell populations in distal respiratory airways (RAs). These populations accumulate in patients with lung injury, chronic obstructive pulmonary disease (COPD) and idiopathic pulmonary fibrosis (IPF). Their lineage potentials and roles are unknown, however. As they are absent in rodents, deeper understanding of these cells requires a human *in vitro* model. Here we report the generation from human pluripotent stem cells (hPSCs) of expandable spheres ('induced respiratory airway progenitors' (iRAPs)) consisting of all RA-associated cell types. iRAPs could differentiate into type 1 (AT1) and type 2 alveolar (AT2) epithelial cells in defined conditions, showing that alveolar cells can be derived from RAs. iRAPs with deletion of HPS1, which causes pulmonary fibrosis in humans, display defects that are hallmarks of IPF, indicating involvement of intrinsic dysfunction of RA-associated cells in IPF. iRAPs thus provide a model to gain insight into human lung regeneration and into pathogenesis of IPF.

INTRODUCTION

The respiratory epithelium consists of basal (BC), ciliated, secretory, goblet and neuroendocrine cells in the airways, and alveolar type 1 (AT1) and surfactant-producing alveolar type 2 (AT2) cells in the alveoli.[1] AT1 cells, through which gas exchange takes place, are the primary cell of the respiratory system, and lung regeneration after injury is geared towards restoring AT1 function. The best characterized mechanism is the conversion of a fraction of AT2 cells to AT1 cells through transitional intermediates,[2–4] although AT1-to-AT2 plasticity exists in the neonatal mouse lung.[5] While most mouse studies on alveolar repair after injury are based on the premise of AT2-to-AT1 conversion, lineage tracing studies have suggested a contribution of cells with characteristics of airway secretory cells after severe injury.[2,6–11] Multiple cellular pathways might therefore converge on alveolar repair.

Putative regenerative cells with features of airway secretory cells have recently also been identified in humans. In contrast to mice, humans, primates and ferrets have 'respiratory airways' (RAs) or 'terminal respiratory bronchioles' (TRBs), representing the most distal branches of airway tree into which individual alveoli open and that terminate in alveolar ducts, where multiple alveoli coalesce. Expression of the secretory cell marker, *SCGB3A2*, was identified in scRNA-seq studies of the distal lung in cells also co-expressing AT1 and AT2 markers.[12] Basil et al. reported presence of *SCGB3A2*$^+$ cells negative for the AT2 marker, *SFPTC*, in RAs.[13] Murthy et al. identified multiple subpopulations in RAs characterized by co-expression of another AT2 marker, *SFTPB* **(Fig. 1a)**.[14] The increased abundance of these populations after lung injury, in COPD and in IPF suggests a role in regeneration.[12–14] We therefore call these cells 'respiratory airway progenitors' (RAPs). In addition to RAPs, IPF lungs also show accumulation of 'aberrant basaloid cells' (aBCs), a population that is much less abundant, though not absent, in normal lungs and expresses *KRT17*, *COL1A1* and other extracellular matrix (ECM) components but lacks common BC markers such as *KRT5*.[12,15]

As they are absent in rodents, insight into the lineage potentials and role of RAPs requires a human *in vitro* model. Here we report the generation from human pluripotent stem cells (hPSCs) of expandable, clonal spheres that consist of all cell populations present in RAs and can differentiate into AT2 and AT1 cells. These ‘induced respiratory airway progenitors’ (iRAPs) display hallmarks of IPF when carrying a mutation associated with familial IPF, thus suggesting a link between intrinsic defects of RAPs and IPF pathogenesis. iRAPs thus provide an *in vitro* model to gain insight into mechanisms underlying normal and pathological human alveolar regeneration and to discover and validate drug targets.

Generation of transitional lung spheres

We previously developed a directed differentiation strategy of hPSCs (embryonic (ESCs) and induced pluripotent stem cells (iPSC)) into 3D lung organoids (LOs) that undergo a process similar to branching morphogenesis.[16,17] We cultured dissociated cells from LOs in medium supplemented with CHIR (GSK3 inhibitor), keratinocyte growth factor (KGF), dexamethasone, 3′,5′-cyclic adenosine monophosphate (cAMP), and 3-isobutyl-1-methylxanthine (IBMX) (CK-DCI) (**Fig. 1b**), previously reported to promote outgrowth of spheres containing AT2 cells (alveolospheres) from hPSC-derived lung progenitors.[18–20] Within 2 weeks, hollow spheres developed (**ESC Fig.1c; iPSC ED1a**) that could be serially passaged every ~3 weeks for up to at least 7 passages with an average expansion of ~10-fold between each passage **(ESC ED2a, iPSC ED1b)**. Generation of spheres from mixtures of LO cells expressing either GFP or mScarlet yielded spheres with only one fluorescent reporter, indicative of clonality (**Fig. 1d**).

scRNA-seq revealed a relatively homogenous population with respect to expression of epithelial (*EPCAM)*, lung (*NKX2.1)*, and AT2/RAP (*SFTPB)* markers (**Fig. 1e**). A large subpopulation expressed *SCGB3A2*, with some *SCGB3A2*$^+$ cells co-expressing AT2 markers (*SFTPC*, *NAPSA* and *ABCA3)* (**Fig. 1e**). The *SCGB3A2*$^-$ population expressed *IGFBP2*, a BC marker according to LungMap (**Fig. 1e**).[21] Murthy et al. described several subpopulations residing in human terminal airways, including *SFPTB*$^+$*SCGB3A2*$^-$ distal BCs, some of which are low to negative for the airway BC markers, *KRT5* and *p63*, *SFTPB*$^+$S*CGB3A2*$^+$*SCGB1A1*$^+$ pre-TRB secretory cells (pre-TRB-SCs), *SFTPB*$^+$S*CGB3A2*$^+$*SFTPC*$^-$ TRB-SCs, and, finally, *SCGB3A2*$^+$*SFTPB*$^+$*SFTPC*$^+$ “AT0” cells near the alveolar sacs **(Fig. 1a)**.[14] Cell type annotation using machine learning trained on these data showed that the *SCGB3A2*$^+$ population consisted of AT0 cells and TRB-SCs, whereas the *SCGB3A2*$^-$*IGPBP2*$^+$ population mapped to distal BCs (**Fig. 1f**). Interspersed between those were ‘differentiating BCs’ and rare ‘immature AT1 cells’, likely representing differentiation intermediates. Except for a small, distinct population of

neuroendocrine cells, no match with any other lung populations was found. Because the spheres contained almost exclusively cells associated with RAs, we called these cells 'induced respiratory airways progenitors' (iRAPs).

Trajectory analysis using scVelo[22] showed differentiation pathways originating from distal BCs and terminating in AT0 cells (**Fig. 1g**). These findings suggest a lineage from distal BCs over TRB-SCs to AT0 cells that was not recognized in recent scRNA-seq studies of human lung but matches the proximodistal arrangement of these cell types *in vivo* **(Fig. 1a)**. Cell identity assignment based on the data of Habermann et al.,[12] which included samples from IPF patients, showed comparable cell identity assignment while also revealing the presence of *KRT5*$^{-}$*KRT17*$^{+}$ aBC-like cells (**Fig. 1h**)

RT-qPCR for *SFTPC*, *SFTPB* and *SCGB3A2* mRNA confirmed the scRNA-seq analysis **(ESC, Fig. 2a; iPSC, ED1c)**. Confocal microscopy revealed uniform expression of EPCAM, NKX2.1 and SFTPB, with pro-SFTPC expressed in some of the spheres **(ESC, Fig. 2b; iPSC, ED1d-e)**. SFTPB and SCGB3A2 were expressed within the same spheres **(ED2b)**. Western Blot showed detectable presence of fully processed SFTPB and SFTPC **(ESC Fig 2c, iPSC ED1f)**. HT2-280, a marker of mature AT2 cells,[23] accounted for ~2% of the cells **(ESC Fig. 2d; iPSC ED1g,** representative gating strategy **ED3**)**.** iRAP spheres showed apical accumulation of the lysosomal dye, LysoTracker Red (**ED2c**) and lamellar bodies (LBs) by transmission electron microscopy (**Fig. 2e, arrows**), a feature of AT2 cells. However, these had low electron density and were often organized as multivesicular bodies, indicative of immaturity.[24] iRAPs maintained a stable phenotype over several passages after passage one (**ED2d**) and were phenotypically similar whether generated from early or late stage LOs (**ED2e**). They can be cryopreserved and thawed while retaining their expression profile (**ED2f**). Together, these observations indicate that iRAP spheres contain a mixture of AT0 cells, TRB-SCs, distal BCs and aBCs, thus encompassing recently identified RAPs in the human distal lung.

Distal specification of iRAPs

We sought to mature iRAP cells into more distal fates by retraction of CHIR, as previous reports showed that CHIR removal induced AT2 maturation of hPSC-derived alveolospheres.[18,19] CHIR removal led to disintegration of the spheres (**ED4a),** decreased proliferation (**ED4b)** and a modest increase of the HT2-280$^+$ fraction (**ED4c**) which was, however, not corroborated by mRNA expression of the AT2 marker, *SFTPC* (**ED4d**). Furthermore, blocking NOTCH signaling using DAPT, shown previously to induce SFTPC expression in SCGB3A2$^+$ cells,[13] did not significantly affect expression of AT2 markers, except for a modest increase in *ABCA3* mRNA (**ED4e-f).**

To gain deeper insight into signaling pathways driving distal differentiation, we took advantage of publicly available scRNA-seq data (https://fetal-lung.cellgeni.sanger.ac.uk/) collected from human embryonic lung at ~16-22 weeks post-conception.[25] Our re-analysis confirmed the presence of a 'lung epithelium' cluster (**ED5a**), containing cells expressing *EPCAM*, *NKX2.1*, *SFTPB*, *SFTPC*, *AGER* and *SCGB3A2* (**ED5b**). This cluster contained 5 distinct subclusters (**ED5c**), two of which were of particular interest: the 'SFTPB$^+$SCGB3A2$^+$' cluster, and the 'AT1-AT2 progenitor' cluster expressing *AGER*, *SFTPB* and *SFTPC* but no *SCGB3A*2 (**ED5d**). Differential gene expression (DEG) analysis showed that genes defining the 'AT1-AT2 progenitor' cluster were affiliated with 'lung' and 'fetal lung' (**ED5e**). Gene Ontology (GO) analysis suggested involvement of TGF-β signaling (**ED5f**) at this stage of development. UMAP feature plots showed increased expression of SMAD6 and SMAD7, negative regulators of TGF-β signaling, and of NOTUM, a negative regulator of WNT signaling previously shown to be involved in alveolar development (**ED5g)**.[26] These data suggested that TGF-β and WNT signaling are downregulated during distal differentiation of *SCGB3A2*$^+$ cells.

To examine whether TGF-β inhibition in the absence of WNT signaling would induce distal differentiation, we cultured iRAPs for 14 days in the presence of DCI and SB-431542, a TGF-β inhibitor[27,28] (DCI-SB, **Fig. 3a,b**). While the AT1 marker, HT1-56,[29] is absent in iRAPs cultured in

CK-DCI and expression of HT2-280 is low, iRAPs cultured with DCI-SB contained ~40% HT1-56$^+$ and ~30% HT2-280$^+$ cells **(ESC Fig. 3c and ED6a, iPSC ED1h-j)**. We therefore call the cells distalized iRAPs (D-iRAPs). As no induction of distal markers was observed with DCI or SB alone **(Fig ED6b-e)**, both are necessary for induction of distal fates. BMP inhibition with NOGGIN did not result in induction of HT1-56 or HT2-280, indicating that iRAP differentiation is specifically driven by inhibition of TGF-β **(Fig. 3c)**. FGF7 and FG10 are dispensable, and even reduced HT2-280 expression **(Fig. 3c)**. RT-qPCR showed increased expression of *SCGB3A2, SFTPC*, *SFTPB* and *AGER* mRNA in D-iRAPs compared to iRAPs (**Fig. 3d**), indicative of a more distal fate. Co-staining for pro-SFTPC and RAGE (the protein encoded by *AGER*) showed that ~27% of spheres were proSFTPC$^+$, 10% were AGER$^+$ and 68% were proSFTPC$^+$RAGE$^+$ (**Fig. 3e,f, ED6f,i**). RAGE and SFTPC were present within the same sphere in 43%, whereas spheres only staining for SFTPC or RAGE represented 27% and 21% of the total, respectively **(Fig. 3e,f, ED6g,h,i)**. scRNA-seq analysis **(Fig. 3g,h)** showed that a large fraction of D-iRAPs expressed *SFTPC*, whereas the highest *SCGB3A2* expression was now found in a population expressing the AT1 markers, *AGER, CLIC5* and *CAV1*, markers that were absent from iRAPs. *ASCL1*$^+$*NEUROD*$^+$ neuroendocrine cells were still present, while *IGFBP2*$^+$ distal BCs became rare **(Fig. 3h)**.

We conclude that removal of WNT signaling and inhibition of TGF-β signaling specifies iRAPs toward alveolar epithelial cells.

Specification of AT1 cells

Expression of AT1 markers and *SCGB3A2* overlapped in D-iRAPs, suggesting incomplete maturation **(Fig. 3h)**. A longer differentiation time in DCI-SB conditions up to 21 days did not enhance maturation but decreased cell viability (**ED6j**). We therefore explored other strategies to obtain mature AT1 cells. Physical forces affect AT1 development, suggesting that their specification may require adherent 2D culture conditions.[5,30,31] Moreover, BMP signaling was previously shown to increase AT1 differentiation efficiency following pneumonectomy in mice,[32] a

finding consistent with our observation that the BMP inhibitor, NOGGIN, negatively impacted the specification of alveolar cell types in iRAPs (**Fig. 3c**). We therefore dissociated D-iRAP spheres and plated the cells on Matrigel-coated plates and subsequently in air-liquid interphase (ALI) cultures. (**Fig. 4a, ED7a**). All cultures were supplemented with ROCK inhibitor which was shown to promote proliferation and survival of airway cells in 2D cultures.[33] While medium supplemented with BMP4 did not allow attachment of the cells (**ED7b**), high expression of RAGE protein and *AGER* mRNA was maintained in the presence of DCI-SB, SB only and BMP4-SB in submerged 2D culture (**ED7c-d**). Interestingly, the combination of BMP4 and SB downregulated SCGB3A2 and SFTPC protein and mRNA (**ED7c-d**), indicative of AT1 at the expense of AT2 maturation. Similarly, in air liquid interface (ALI) conditions, cells cultured in BMP4-SB maintained confluency (**ED7e-f)**, *AGER*/RAGE **(Fig. 4b-d)** and HT1-56 **(Fig. 4e)** expression but lost expression of *SFTPC* and *SCGB3A2* mRNA (**Fig. 4b)** and protein **(Fig. 4c-d)**. More than 95% of the cells expressed HT1-56, whereas HT2-280 became undetectable **(Fig. 4e**). Some *SFTPB* mRNA and protein were still detected however **(ED7g)**. Co-localization analysis showed that SFTPB$^+$ cells only accounted for ~6% of RAGE staining, indicative of an overall mature AT1 lineage (**ED7h,i).** ScRNA-seq analysis showed that >90% of the cells were classified as AT1 cells **(Fig. 4f)**. We call these cells induced AT1 (iAT1) cells. A minor fraction was identified as AT2, whereas a small cluster co-expressed *SCGB3A2* and *SFTPC*, indicative of AT0 identity (although query of the Human Lung Cell Atlas[34] spuriously classified the cells as 'secretory' and 'macrophages') **(Fig. 4f).** Taken together, iAT1 maturation requires inhibition of TGF-β and activation of BMP signaling in both submerged and ALI 2D conditions.

Merged analysis of scRNA-seq data from the iRAPs, D-iRAPs and iAT1 cells **(Fig. 5a**) confirmed acquisition of the AT1-AT2 markers during the transition from iRAPs to D-iRAPs and maturation of AT1 cells with loss of *SFTPC* and *SCGB3A2* in the iAT1 stage, where *AGER*$^+$*CAV1*$^+$ cells are predominant. **(Fig. 5b-d**). Proximal lung and digestive tract markers were absent at each

stage of the development **(Fig. 5d**). Bulk RNAseq comparing cells at the iRAP, D-iRAP and iAT1 stage of the differentiation protocol **(Fig. 5a)** led to similar conclusions **(Fig. 5e,f; ED8a)**. There were 2909 differentially expressed genes between iRAPs and iAT1 cells, and 2821 between D-iRAPs and iAT1 cells stages (**ED8b**, **Source Data 2**). Gene ontology (GO) analysis showed significant induction of the terms, 'cell shape', 'actin filaments' and 'cell junctions' consistent with extensive remodeling of cell morphology during AT1 differentiation **(Fig. 5g; ED8c-d).** Furthermore, the 'HIPPO signaling' pathway, which is essential for the generation of AT1 cells during development and after injury in mice,[35–37] was a significantly induced pathway **(Fig. 5g,h)**. Interaction analysis using String-DB[38] showed that DEGs involved in regulation of actomyosin cytoskeleton and cell junctions were connected to Hippo signaling **(Fig. 5i, ED8e)**, consistent with the reported crosstalk between small GTPase and Hippo signaling[39] and with the role of CDC42 in epithelial morphogenesis[40] and acquisition and maintenance of AT1 identity.[5,31,35]

iRAPs with mutation associated with IPF display hallmarks of IPF

Although injury to AT2 cells is considered critical to IPF pathogenesis,[41] we examined whether iRAPs with a mutation associated with IPF would show intrinsic abnormalities, as they share the presence of LBs and expression of SFTPB with AT2 cells. We generated iRAPs from ESCs with targeted deletion of Hermansky-Pudlak Syndrome (HPS)1. HPS is caused by abnormal trafficking of lysosome-related organelles (LROs) due to mutation in one of 11 HPS genes and share pigmentation abnormalities and platelet dysfunction, as both melanosomes and platelet delta granules are LROs.[42] Some HPS mutations (HPS1, 2 and 4) are fully penetrant for HPS-associated interstitial pneumonia (HPSIP), an entity considered clinically indistinguishable from IPF.[43] IPF in patients with HPS is likely caused by abnormal biogenesis and trafficking of LBs, which are also LROs. We showed previously that mutation of *HPS1* induced extensive fibrosis in hPSC-derived LOs.[16,44]

scRNA-seq of WT and *HSP1*$^{-/-}$ iRAPs **(Fig. 6a)** showed similar presence of *NKX2.1* and *SFTPB* with a small fraction of *SFTPC*$^{+}$ cells in both genotypes **(Fig. 6b)**. Similar expression of distal lung markers was also confirmed by RT-qPCR **(ED9a)**. *HPS1*$^{-/-}$ iRAPs, however, contained more cells expressing *KRT17*, *COL1A1* and *COL3A1* **(Fig. 6b)**, which was confirmed by RT-qPCR **(Fig. 6c)**, a phenotype consistent with aBC-like cells. The doubling time of *HPS1*$^{-/-}$ iRAPs was shorter compared to parental WT iRAPs in later passages, a finding potentially consistent with their accumulation in IPF **(ED9b)**. Lysotracker Red fluorescence was reduced in *HPS1*$^{-/-}$ compared to WT iRAPs **(Fig. 6d, ED9c)**, indicative of dysfunction of the lysosomal/endolysosomal compartment (which includes LBs). Given the potential role of ER stress in IPF,[41] we assessed the unfolded protein response of the ER (UPR^{ER}). Addition of tunicamycin, an inhibitor of glycosylation that induces ER stress, increased *XBP1* splicing **(Fig. 6e)**, BIP expression **(Fig. 6f)**, and apoptosis **(Fig. 6g, ED9d)** in *HPS1*$^{-/-}$ compared to WT iRAPs, indicative of increased ER stress susceptibility.

At the D-iRAP stage **(Fig. 6h)**, differentiation of *HPS1*$^{-/-}$ cells was impaired especially into the AT1 lineage as evidenced by a reduced fraction of HT1-56^{+} cells **(Fig. 6i)** and a sharp reduction in *AGER* expression (**Fig. 6j)**. In the AT2 lineage, a decrease in HT2-280^{+} cells was noted **(ED9e),** but expression of other AT2 markers, *LAMP3*, *SFTPB* and *SFTPC,* was not significantly affected **(ED9f)**. At the iAT1 stage **(Fig. 6k)**, *HPS1*$^{-/-}$ cells, while uniformly expressing HT1-56 **(ED9g,h)**, showed a decrease in HT1-56 mean fluorescence intensity **(Fig. 6l)** and a striking reduction in *AGER* mRNA **(Fig. 6m)** compared to WT, indicative of a differentiation or maturation defect.

We conclude that *HPS1*$^{-/-}$ iRAPs display phenotypes corresponding to abnormalities observed in IPF, suggesting that intrinsic defects in RAPs play a role in the pathogenesis.

DISCUSSION

The iRAPs described here consist of populations identified in human terminal airways, and also include cells classified as aBCs, which are mainly, but not exclusively observed in IPF.[12,15] iRAPs can be differentiated into AT1 cells in defined conditions, and show abnormalities that are hallmarks of IPF when mutant for HPS1, thus providing important novel insights into pathogenesis of fibrotic lung disease.

Published data on the lineage relations among RAPs are conflicting. scVelo analysis of iRAPs suggests that distal BCs are the progenitors and AT0 cells the most mature population, a differentiation trajectory that aligns with the reported proximodistal location of the corresponding populations *in vivo* **(Fig. 1a)**.[14] Basil et al. identified, using a reporter gene, SCGB3A2$^+$ cells in airway organoids that lost SCGB3A2 and acquired AT2 markers when cultured in CK-DCI.[13] In our hands, however, these conditions maintained SCGB3A2 expression and prevented AT1 and AT2 maturation. The reasons for this discrepancy are unclear. Murthy et al., on the other hand suggested, based on trajectory analysis and studies in organoids generated from adult lungs, that AT0 cells are intermediates between AT2 and AT1 cells and can also give rise to TRB-SCs. Trajectory analysis by Habermann et al.[12] suggested that *SCGB3A2*$^+$ cells can be upstream of transitional AT2 cells expressing AT1 and AT2 markers, which are precursors of AT1 and AT2 cells, a hierarchy most compatible with our observations. It is likely that, given the well-established lineage plasticity occurring during lung regeneration,[1,12] multiple distal cell types can give rise to AT1 cells during injury repair through context-dependent differentiation trajectories.

In addition to representing a model to study human distal lung regeneration, iRAPs also allow dissection of AT1 differentiation in defined conditions. This notion is supported by network analysis of DEGs during iAT1 induction, which revealed coordinated regulation of the actomyosin cytoskeleton and Hippo signaling. CDC42, a key regulator of the actomyosin cytoskeleton,[40] induces and maintains AT1 identity in response to mechanical stress.[5,31] Hippo signaling is

involved in AT1 differentiation after various forms of injury including bleomycin, LPS, bacterial infection and unilateral pneumonectomy,[30,36,36,37] and its downstream transcriptional regulators, YAP and TAZ, are regulated by mechanical stress and RhoGTPases.[36,37] It is interesting to note that pathways involved in translation were downregulated during iAT1 generation **(ED8d)**, suggesting a role for translational regulation in AT1 differentiation that was not recognized before.

iRAPs with deletion of HPS1 display functional defects, including hyperresponsiveness to ER stress, increased expansion and impaired differentiation with increased presence of aBC-like cells. These findings align with results of scRNAseq studies of IPF lungs showing depletion of AT1 and AT2 cells and accumulation of aBCs,[12,15] and suggest that, although susceptibility to AT2 injury is a factor in IPF pathogenesis,[41] intrinsically aberrant injury repair by the distal lung progenitor compartment may play a major role as well. In particular the AT1 differentiation defect coupled with increased aBC-like cells observed in iRAPs may be important, as regions in IPF lungs with accumulated aBC-like cells lacked RAGE^{+} AT1 cells.[3] Furthermore, a reduction of soluble RAGE in the serum is a biomarker for IPF, potentially because of the striking depletion of AT1 cells.[45] A role for AT1 depletion in the pathogenesis of IPF is also suggested by the observation that impairment of AT1 differentiation by deletion of CDC42 after unilateral pneumonectomy in mice resulted in fibrosis with a pattern similar to that of IPF.[31] A role for RAPs in IPF would also explain why short telomeres are the most important risk factor for IPF, as telomere dysfunction primarily affects proliferative stem cell compartments.[46] The fact that iRAPs contain LBs and express SFTPB suggests that mechanisms involved in impaired cellular maintenance and susceptibility to injury of AT2 cells[41] affect these regenerative populations as well.

In conclusion, the generation of iRAPs from hPSCs allowed the development of the first protocol to generate AT1 cells from hPSCs in defined conditions and to show that not only AT2 cells, but distal lung progenitors are intrinsically dysfunctional in IPF, shedding a new light on

pathogenesis and providing a versatile tool for drug discovery.

Methods

Human lung samples.

De-identified normal human lung samples were provided by the Herbert Irving Comprehensive Cancer Center Molecular Pathology Shared Resource Tissue Bank core under IRB-AAAT8682.

Maintenance of hPSCs

Before differentiation, Rockefeller University Embryonic Stem Cell Line 2 (RUES2, passage 24-32) or mRNAi PSC lines (generated using mRNA transfection and obtained from the Mount Sinai Stem Cell Core, NY) were maintained on mouse embryonic fibroblasts (MEFs) plated at 22,500 cells/cm^2. Cells were cultured in hESC maintenance media (DMEM/F12 (ThermoFisher, Carlsbad, CA), 20% Knock-out serum, (Stem Cell Technologies, Vancouver, BC), 0.1 mM β-mercaptoethanol (Sigma-Aldrich,Burlington, MA) , 0.2% Primocin (InvivoGen, San Diego, CA), 20 ng/ml FGF2 (R&D Systems/Biotechne, Minneapolis, MN), and 1% Glutamax (ThermoFisher)) which was changed daily. hPSCs were passaged every 3-4 days with Accutase (Innovative Cell Technologies, San Diego, CA) at least two times before differentiation, washed and replated at a dilution of 1:24. Cultures were maintained in a humidified 5% CO_2 atmosphere at 37°C. Lines are karyotyped and verified for Mycoplasma contamination using PCR (InVivoGen) every 6 months.

Generation of hESC-derived lung organoids

Human LOs were generated as described previously. Briefly, MEFs were depleted by passaging 5-7x10^6 hESCs onto Matrigel (Corning, Corning, NY) coated 10-cm dish. Cells were maintained in hESC media in a humidified 5% CO_2 atmosphere at 37°C. After 24 hours, cells were detached with 0.05% Trypsin/EDTA (ThermoFisher) and distributed to 6-well low-attachment plates containing primitive streak/embryoid body media (10 μM Y-27632 (Tocris/Biotehne, Minneapolis, MN), 3 ng/ml BMP4 (R&D/Biotechne) to allow embryoid body (EB) formation. EBs were fed every day with fresh endoderm induction media (10 μM Y-27632, 0.5 ng/ml BMP4, 2.5 ng/ml FGF2 and

100 ng/ml ActivinA (R&D/Biotechne)) and maintained in a humidified 5% CO_2/5% O_2 atmosphere at 37°C. Endoderm yield was determined by dissociating EBs and evaluating CXCR4 and c-KIT (Biolegend, San Diego, CA) co-expression by flow cytometry on day 4. Cells used in all experiments had > 90% endoderm yield and were plated on 0.2% fibronectin-coated wells (R&D/Biotechne) at a density of 80,000 cells/cm^2. Cells were incubated in Anteriorization media-1 (100 ng/ml Noggin (R&D/Biotechne) and 10 μM SB431542 (Tocris)) for 24 hours, followed by Anteriorization media-2 (10 μM SB431542 (Tocris) and 1 μM IWP2 (Tocris)) for another 24 hours. At the end of anterior foregut endoderm induction, cells were switched to Ventralization/Branching media (3μM CHIR99021 (Tocris), 10 ng/ml FGF10 (R&D/Biotechne), 10 ng/ml rhKGF, (R&D/Biotechne), 10 ng/ml BMP4 and 50 nM *all-trans* Retinoic acid (Tocris)) for 48 hours and three-dimensional clump formation was observed. The adherent clumps were detached by gentle pipetting and transferred to the low-attachment plate, where they folded into lung bud organoids (LBOs) at d10-d12. Branching media was changed every other day until d20–d25 and LBOs were embedded in 100% Matrigel in 24-well transwell (BDFalcon, Franklin Lakes, NJ) inserts. Branching media was added after Matrigel solidified and changed every 2-3 days to facilitate proper growth into lung organoids. Culture of embedded organoids can be kept for more than 6 months.

Generation of induced respiratory airway progenitors (iRAP)

Matrigel embedded lung organoids can be used for iRAP generation when they reach d42 of development. Media was removed from the transwell and 1 ml of 2 mg/ml dispase (Corning) was added to release lung organoid from the Matrigel for 30-45 minutes in a normoxic incubator. The organoid was transferred to a 15 ml conical tube and washed with stop media (DMEM (Corning), 5% FBS (Atlanta Biologicals; Flowery Branch, Georgia), 1% Glutamax (ThermoFisher)) to neutralize dispase, then centrifuged at 200 g for 5 minutes. The pellet was incubated with 1 ml of 0.05% Trypsin/EDTA in a normoxic incubator for 10-12 minutes with occasional pipetting with a

P1000 pipet tip. Single cell dissociation was verified using a bright field microscope. If a single cell suspension was not obtained after 12 minutes, cells were washed with stop media and incubated for additional 5 minutes with 0.05% Trypsin/EDTA. Cells were counted using a hemocytometer and 400 cells/µl of undiluted Matrigel were plated in a well of a 12-well non-tissue culture plate. The plate was placed in normoxic incubator for 30 minutes until Matrigel polymerized and 1 ml of CK-DCI (3µM CHIR 99021, 10 ng/ml rhKGF, 50 ng/ml dexamethasone (ThermoFisher), 0.1 mM 8-Bromoadenosine 3′,5′-cyclic monophosphate sodium salt (Tocris) and 0.1 mM 3-Isobutyl-1-methylxanthine (Sigma-Aldrich)) media was gently added using 10 ml serological pipette. Media was changed every 3 days. After 2-3 weeks, an iRAP culture is established that can be maintained for at least 8 passages.

Generation of D-iRAPs

7-10 days after passaging, small iRAP spheres formed. CK-DCI media was replaced with DCI-SB ((50 ng/ml dexamethasone (ThermoFisher), 0.1 mM 8-Bromoadenosine 3′,5′-cyclic monophosphate sodium salt (Tocris) and 0.1 mM 3-Isobutyl-1-methylxanthine (Sigma-Aldrich), 10 µM SB-431542 (Tocris)) for 10-14 days.

Generation of iAT1 cells

6-well transwell inserts (BDFalcon, Franklin Lakes, NJ) were coated with 1:15 Matrigel:SB-BMP4-RI (10 µM SB-431542 (Tocris), 10 ng/mL BMP4 (Tocris), and 10 µM Y-27632 (Tocris)) and left at 4°C overnight. Mature D-iRAPs were released from Matrigel using dispase and washed, as described above. Media was aspirated from the transwell when ready to seed with cells. 2.5 x 10^5 cells were resuspended in 1 mL of SB-BMP4-RI and added into the insert. 1-2 mL of SB-BMP4-RI was added into the 6 well. The cells were cultured for 5-7 days in a normoxic incubator at 37°C. For ALI, 7 days after seeding on the transwell insert, the media in the insert was removed and the cells were incubated for another 4-5 days.

RT-qPCR.

Total RNA was extracted according to manufacturer's instructions using the Direct-zol™ RNA Microprep (Zymo Research, Irvine, CA) and 500 ng of total RNA was reverse transcribed using the qScript™ XLT cDNA SuperMix (Quantabio, Beverly, MA). Technical triplicates of 15 µl reaction (for use in Applied Biosystems QuantStudio7 384-well System, Waltham, MA) were prepared with 3 µl of diluted cDNA and run for 40 cycles. Primers used are listed in **Table S1**. Relative gene expression was calculated based on the average cycle (Ct) value, normalized to *GAPDH* as the internal control and reported as fold change (2(-ddCT)).

Immunofluorescence.

After removal of media, a cell scraper was used to carefully detach the Matrigel droplet with embedded IRAPs from the bottom of the 12 well plate. The droplet was then transferred to an OCT histology mold and embedded in Tissue-Tek OCT (Sakura Finetek, Torrance, CA). Frozen samples were cut using a cryotome at the thickness of 10-12 µm and collected on adhesion microscope slides, air-dried and fixed in 4% paraformaldehyde, then washed 2 times for 5 minutes in 50 mM glycine to inactivate PFA, followed by washing in PBS. Samples were permeabilized for 10 minutes in 0.2% PBST (PBS + 0.2% Triton X-100 (Fisher Scientific, Hampton, NH)) and blocked by incubating in PBS containing 5% donkey serum, then incubated overnight in primary antibody **(Table S2)** in 0.2% Triton X-100 and 2% donkey serum. On the next day, samples were washed three times in PBS and 1% donkey serum and incubated with secondary antibodies (1:200, **Table S2**) for 1 hour at room temperature. Nuclei were stained with DAPI (ThermoFisher) and sections were mounted with Mounting Reagent (DAKO, Santa Clara, CA) on coverslips. Samples were imaged using a Leica TCS SP8 Stellaris Laser scanning confocal microscope, and Leica DMi1 Inverted Phase Contrast Microscope (Leica Microsystems, Deerfield, IL).

3D imaging

Tips and conical 15 ml plastic tubes were pre-coated with 1% (wt/vol) PBS–BSA. D-iRAPs were released from Matrigel as previously described in the 'Generation of induced Respiratory Airway Progenitor' section. Spheres were transferred into a precoated 15 ml falcon tube with ice cold 1% (wt/vol) PBS–BSA. Tubes were centrifuged at 70g for 3 min at 4°C. Pellets were resuspended in ice cold 4% PFA with precoated tips and incubated for 10 min. 15 ml conical plastic tubes were filled with PBT (PBs-Tween: 0.1% (wt/vol) Tween 20 in PBS) for 10 min at 4°C on roller rotation. Spheres were centrifuged at 70g for 3 min at 4°C and resuspended with ice cold 1% (wt/vol) PBS–BSA for 45 min at 4°C on roller rotation. Staining procedure followed the same step as described in the 'Immunofluorescence' section, albeit both primary and secondary antibodies were incubated overnight at 4°C on roller rotation. Mounting was performed on a glass slide, between two coverslips. Imaging was performed on a Leica TCS SP8 Stellaris Laser scanning confocal microscope. Z-stacks were acquired every ~700 nm, covering the height of each sphere.

Image processing

The 3D reconstituted images were analyzed using Aivia software version 12.0.0. The intensity detection threshold for each signal was set using iRAPs signal intensity. Surfaces were created for DAPI, AGER, proSFTPC and SFTPC signals. Surface parameters consisted of an image smoothing filter size of 9, a minimum edge intensity of 30 and a partition radius of 20 µm. Surface measurements were collected and normalized to control conditions. 2D images were processed using ImageJ version 2.1.0/1.53c.

ER stress

CK-DCI media was replaced with CK-DCI plus 5 µg/mL tunicamycin (Sigma-Aldrich) and returned to a normoxic incubator for 5 hours. Cells were then collected for mRNA analysis. For apoptosis studies, CK-DCI media was replaced with CK-DCI plus 0.1 µg/mL tunicamycin (Sigma-Aldrich) and returned to a normoxic incubator for 5 days. Cells were then released and prepared for cell-cycle analysis (see below).

Lysotracker uptake

CK-DCI media was replaced with CK-DCI plus Lysotracker Red DND-99 (Thermofisher) at a concentration of 75 nM and returned to a normoxic incubator for 2.5 hours. Cells were kept in Matrigel and imaged using Leica DMi1 Inverted Phase Contrast Microscope (Leica Microsystems, Deerfield, IL) and then released from Matrigel for flow cytometric analysis.

Flow cytometry

Spheres embedded in Matrigel were released by incubating with dispase for 30-60 minutes, then washed and dissociated into single cells with 0.05% Trypsin/EDTA in a normoxic incubator for 10-12 minutes with occasional pipetting with a P1000 tip. The single cell suspension was stained in polystyrene round-bottom 12 x 75 mm tubes (BD Falcon). Primary HT1-56 (Terrace Biotech, San Francisco, CA, 1:200 dilution) and HTII-280 (Terrace Biotech, San Francisco, CA, 1:200 dilution) antibodies were incubated for 1 hour at room temperature. Cells were washed two times with FACS buffer (PBS, 1% BSA) and centrifuged for 5 minutes at 1400 rpm. Fluorochrome-labeled secondary antibody (Alexa Fluor 488 #A21042, or 594 #A21044 goat anti-mouse IgM, Thermofisher) were diluted in FACS buffer at 1:100 and added for 30 minutes in the dark. Cells are washed twice. Conjugated human EPCAM antibody (Biolegend) was added for 30 minutes. Cells were washed and resuspended in FACS buffer for flow cytometric analysis on a ZE5 cell analyzer (Bio-Rad, Hercules, CA) or a Novocyte Quanteon (Agilent, Santa Clara, CA).

Cell Cycle Analysis

Single-cell suspensions were prepared as described above. Single cells were resuspended in 200 µL PBS and ethanol-fixed by adding 800 µl of ice-cold 100% ethanol drop-wise while gently vortexing. Cells were left in fixative for at least 2 hours. Fixed cells were washed in 2 mL PBS 2x after which 200 µL of freshly made propidium iodide solution (.1% Triton-X 100 (Fisher Scientific),

50 µg/mL propidium iodide (Thermo Scientific), 0.2 mg/mL RNAse A (Thermo Scientific) in PBS) was added. Samples were incubated at 37°C for 20 min before flow cytometric analysis.

Transmission Electron Microscopy

Transmission Electron Microscopy (TEM) was performed at the NYU Langone Medical Center Microscopy Core. iRAPs were fixed with 2% paraformaldehyde and 2.5% glutaraldehyde in 0.1M sodium cacodylate buffer (pH 7.2) for 2 hours and post-fixed with 1% osmium tetroxide for 1.5 hours at room temperature, then processed in a standard manner and embedded in EMbed 812 (Electron Microscopy Sciences, Hatfield, PA). Semi-thin sections were cut at 1 µm and stained with 1% Toluidine Blue to evaluate the quality of preservation and find the area of interest. Ultrathin sections (60 nm) were cut, mounted on copper grids and stained with uranyl acetate and lead citrate by standard methods. Stained grids were examined under Philips CM-12 electron microscope and photographed with a Gatan (4k ×2.7k) digital camera (Gatan, Inc., Pleasanton, CA).

Western Blot

Cells embedded in Matrigel were released by incubating with dispase (Corning) for 30 minutes. Cells were washed, collected in PBS, and lysed in lysis buffer (RIPA buffer, 1x Roche Complete Protease inhibitor cocktail, and Roche PhosSTOP). Buffer-treated cells were mechanically lysed using a 25-gauge needle and left on ice for 30 minutes. Human lung samples were homogenized with stainless steel beads and left on ice in the lysis buffer for 4-6 hours. Samples were centrifuged at 15,000 g for 10 minutes and the supernatant was collected and stored at -80°C until analysis. Protein concentration was measured using the Pierce BCA Protein Assay Kit (ThermoFisher). A total of 18 µg of iRAP, hPSC, and human lung lysate were loaded for mature SFTPC analysis and a total of 5 µg of each were loaded for mature SFTPB analysis. Lysates were resolved on pre-cast NuPage 4-12% Bis-Tris gels (Invitrogen) and transferred to nitrocellulose membranes (Bio-Rad, Hercules, CA). The following primary antibodies were used to probe the blots: mature

SFTPC (1:1000, Seven Hills Bioreagents, Cincinatti, OH), mature SFTPB (1:1000, Seven Hills Bioreagents), GAPDH (1:5000, Cell Signaling Technology). Species-specific secondary antibodies with HRP conjugates (Cell Signaling Technology, Danvers, MA) were used at 1:15,000 dilution. Blots were n treated with Pierce ECL Western Blotting Substrate and visualized using the Amersham ImageQuant 800 (Cytiva, Marlborough, MA).

Cryopreservation of iRAPs

2-3 weeks after iRAPs were passaged, CK-DCI media was removed and 1 mL of dispase (2 mg/mL) released the spheres. After 30-45 minutes in a normoxic incubator, the spheres were transferred to a 15 mL conical and washed with wash media, then centrifuged at 200 g for 5 minutes. Wash media was aspirated and the pellet was incubated with 1 mL of 0.05%Trypsin/EDTA in a normoxic incubator for 10-12 minutes. They were washed again, followed by resuspension of the pellet in a small volume of CK-DCI media. Cells were frozen at a density of $5x10^5$ to 10^6 single cells. Cells are resuspended in equal volumes of CK-DCI media and 2x DMSO freezing medium (Quality Biological, Gaitersburg, MD), transferred to a cryovial, and placed in a container that allows a freezing rate of -1°C/min in a -80°C freezer. The next day, cells were transferred to liquid nitrogen. When ready to use, the cryovial is placed in a 37°C water bath until thawed. Cells are transferred to a 15 mL conical tube and washed with wash media, centrifuged at 200 g for 5 minutes, and aspirated. The ideal initial reseeding density is 800 - 1,600 cells per µL of undiluted Matrigel.

RNA-seq and data analysis

Total RNA was extracted from iRAPs, D-iRAPs and iAT1 samples using Qiagen RNA extraction kit according to the manufacturer's instructions. RNA quality was evaluated by Agilent 2100 BioAnalyzer. RNA-seq libraries were prepared and sequenced by the JP Sulzberger Columbia Genome Center High-Throughput Screening Center at Columbia University. Paired-end equencing was performed on a NovaSeq 6000 platform. RNA-seq read quality assessment was

performed using fastQC v.0.12.0. Processed reads were mapped against the human genome (GRCh38.p14) using Gencode v44. The number of reads per gene was counted using Salmon v.1.10.12 providing the count matrix. Differential gene expression was analyzed using DESeq2 v.1.30.1 R package Differentially expressed genes were identified for our study by setting a cutoff of pValue < 1*10^-10 and a fold-change > ±2. Gene ontology analysis was performed using the differentially expressed genes with enrichplot package v.1.10.2, using genome-wide annotation for human database v.3.12.0. Genes contributing to GO terms were fed into String-DB software to perform the protein network analysis according to the pipeline described in ED7e.

Single-cell cDNA library preparation and scRNA-seq

Samples were released from Matrigel using dispase and dissociated into single cells using trypsin. For the multiplexing experiment, dissociated D-iRAPS and iAT1 were tagged using TotalSeq-B anti-human hashtags. The viability of single cells was assessed using Trypan Blue staining, and debris-free suspensions of >80% viability were deemed suitable for single-cell RNA Seq. sc-RNA-seq was performed using the Chromium platform (10x Genomics, Pleasanton, CA) with the 3' gene expression (3' GEX) V3 kit, using an input of ~10,000 cells. Briefly, Gel-Bead in Emulsions (GEMs) were generated on the sample chip in the Chromium controller. Barcoded cDNA was extracted from the GEMs by Post-GEM RT-cleanup and amplified for 12 cycles. Amplified cDNA was fragmented and subjected to end-repair, poly A-tailing, adapter ligation, and 10X-specific sample indexing following the manufacturer's protocol. Libraries were quantified using Bioanalyzer (Agilent) and QuBit (Thermofisher) analysis and were sequenced in paired end mode on a NovaSeq instrument (Illumina, San Diego, CA) targeting a depth of 50,000-100,000 reads per cell.

scRNA-seq computational analysis

Sequencing data were aligned and quantified using the Cell Ranger Single-Cell Software Suite (version 6.1.2, 10x Genomics) against the provided GRCh38 (Ensembl 98) human reference

genome. All further computational analysis of scRNA-seq data was performed using R version 4.1.3 (*https://www.R-project.org/.)* unless otherwise stated.

QC and processing

The aligned data was imported and processed using the R package Seurat v4.1.1[38]. Quality control for doublets and low-quality cells was achieved through exclusion of cells with less than 500 or more than 9000 transcripts and those with a higher than 20% mitochondrial gene contribution, respectively. Additionally, transcripts were retained if they counted over 0 in more than 0.5 % of all cells, otherwise excluded. Count data was then log-normalized and transcripts were scaled and centered, using built-in Seurat functions. Variable transcripts were calculated based on standardized feature values using observed mean and expected variance of a local polynomial regression model. On the resulting variable transcripts 50 principal components were computed, which in turn were used as input for uniform manifold approximation and projection (UMAP) dimensionality reduction. For clustering analysis, a shared nearest neighbor (SNN) graph was constructed and the modularity function optimized using the Leiden algorithm.

Cell type annotation

Potential cell types present in our dataset were predicted through machine learning. In brief, a random forest classifier (SingleCellNet R package)[47] was trained on fully annotated published data by Murthy et al.[14] and Haberman et al.[12] and assessed on a withheld subset. This classifier was then applied to the current dataset and a matching cell type was predicted for each cell. Azimuth-based cell type identification using Human Lung Cell Atlas[34] was used for iAT1 samples.

RNA velocity

RNA velocity was calculated in python using the packages Velocyto and scVelo, according to the developer's manual Briefly, ‘.loom’ files containing both exon and intron information were created from aligned raw data using Velocyto. scVelo was then used to normalize the data and compute

moments. Subsequently, RNA velocity was estimated and projected onto Seurat-derived UMAP coordinates. The length and coherence of the velocity vectors, which indicate differentiation speed and directional confidence, respectively, were calculated. Finally, a dynamical model was applied to analyze transcriptional states and cell-internal latent time and subsequently recompute RNA velocities. The latent time, based solely on the transcriptional dynamics of a cell, was thereby determined.

Statistical analysis

Statistical analysis was performed using unpaired two-tailed Student's t-test, one-way ANOVA, or two way-ANOVA where appropriate using Prism 9. Results are shown mean ± SD. P-values < 0.05 were considered statistically significant. N-value refers to biologically independent replicates, unless noted otherwise.

Acknowledgments:

This work was supported by grants NIH HL120046 (HWS), NIH 1U01HL134760 (HWS), NIH S10 OD032447 (HWS), and NIH T32GM145440 (JAT). This research was also funded in part through the NIH/NCI Cancer Center Support Grant P30CA013696 and used the Tissue bank part of the Molecular Pathology Shared Resource.

Author Contributions

MGP and JAT have performed most of the experiments and analysis, IML developed the generation of iRAPs, JWM oversaw microscope analysis. TAT and NS performed scRNA-seq analysis. KGB and HWS supervised scRNA-seq work and analysis. HWS provided concept, supervised and wrote the manuscript.

Competing interests

HWS, IML and MGP have filed a provisional patent application on the generation of iRAPs. The other authors declare no competing interests.

Data accessibility

Bulk and single cell RNAseq data have been deposited in the GEO database, accession GSE245723: Reviewer's token atcvgyyyrbwtjsv.

1. Basil, M. C. *et al.* The Cellular and Physiological Basis for Lung Repair and Regeneration: Past, Present, and Future. *Cell Stem Cell* **26**, 482–502 (2020).
2. Strunz, M. *et al.* Alveolar regeneration through a Krt8+ transitional stem cell state that persists in human lung fibrosis. *Nat Commun* **11**, 3559 (2020).
3. Kobayashi, Y. *et al.* Persistence of a regeneration-associated, transitional alveolar epithelial cell state in pulmonary fibrosis. *Nat Cell Biol* **22**, 934–946 (2020).
4. Barkauskas, C. E. *et al.* Type 2 alveolar cells are stem cells in adult lung. *J Clin Invest* **123**, 3025–3036 (2013).
5. Shiraishi, K. *et al.* Biophysical forces mediated by respiration maintain lung alveolar epithelial cell fate. *Cell* **186**, 1478-1492.e15 (2023).
6. Choi, J. *et al.* Release of Notch activity coordinated by IL-1β signalling confers differentiation plasticity of airway progenitors via Fosl2 during alveolar regeneration. *Nat Cell Biol* **23**, 953–966 (2021).
7. Choi, J. *et al.* Inflammatory Signals Induce AT2 Cell-Derived Damage-Associated Transient Progenitors that Mediate Alveolar Regeneration. *Cell Stem Cell* **27**, 366-382.e7 (2020).
8. Kathiriya, J. J., Brumwell, A. N., Jackson, J. R., Tang, X. & Chapman, H. A. Distinct Airway Epithelial Stem Cells Hide among Club Cells but Mobilize to Promote Alveolar Regeneration. *Cell Stem Cell* **26**, 346-358.e4 (2020).
9. Kim, C. F. B. *et al.* Identification of bronchioalveolar stem cells in normal lung and lung cancer. *Cell* **121**, 823–835 (2005).
10. Liu, Q. *et al.* Lung regeneration by multipotent stem cells residing at the bronchioalveolar-duct junction. *Nat Genet* **51**, 728–738 (2019).
11. Guha, A., Deshpande, A., Jain, A., Sebastiani, P. & Cardoso, W. V. Uroplakin 3a+ Cells Are a Distinctive Population of Epithelial Progenitors that Contribute to Airway Maintenance and Post-injury Repair. *Cell Rep* **19**, 246–254 (2017).

12. Habermann, A. C. *et al.* Single-cell RNA sequencing reveals profibrotic roles of distinct epithelial and mesenchymal lineages in pulmonary fibrosis. *Sci Adv* **6**, eaba1972 (2020).
13. Basil, M. C. *et al.* Human distal airways contain a multipotent secretory cell that can regenerate alveoli. *Nature* **604**, 120–126 (2022).
14. Kadur Lakshminarasimha Murthy, P. *et al.* Human distal lung maps and lineage hierarchies reveal a bipotent progenitor. *Nature* **604**, 111–119 (2022).
15. Adams, T. S. *et al.* Single-cell RNA-seq reveals ectopic and aberrant lung-resident cell populations in idiopathic pulmonary fibrosis. *Sci Adv* **6**, eaba1983 (2020).
16. Chen, Y.-W. *et al.* A three-dimensional model of human lung development and disease from pluripotent stem cells. *Nat Cell Biol* **19**, 542–549 (2017).
17. Matkovic Leko, I. *et al.* A distal lung organoid model to study interstitial lung disease, viral infection and human lung development. *Nat Protoc* **18**, 2283–2312 (2023).
18. Jacob, A. *et al.* Derivation of self-renewing lung alveolar epithelial type II cells from human pluripotent stem cells. *Nat Protoc* **14**, 3303–3332 (2019).
19. Jacob, A. *et al.* Differentiation of Human Pluripotent Stem Cells into Functional Lung Alveolar Epithelial Cells. *Cell Stem Cell* **21**, 472-488.e10 (2017).
20. Yamamoto, Y. *et al.* Long-term expansion of alveolar stem cells derived from human iPS cells in organoids. *Nat Methods* **14**, 1097–1106 (2017).
21. Sun, X. *et al.* A census of the lung: CellCards from LungMAP. *Dev Cell* **57**, 112-145.e2 (2022).
22. Bergen, V., Lange, M., Peidli, S., Wolf, F. A. & Theis, F. J. Generalizing RNA velocity to transient cell states through dynamical modeling. *Nat Biotechnol* **38**, 1408–1414 (2020).
23. Gonzalez, R. F., Allen, L., Gonzales, L., Ballard, P. L. & Dobbs, L. G. HTII-280, a biomarker specific to the apical plasma membrane of human lung alveolar type II cells. *J Histochem Cytochem* **58**, 891–901 (2010).
24. Chi, E. Y. The ultrastructural study of glycogen and lamellar bodies in the development of fetal monkey lung. *Exp Lung Res* **8**, 275–289 (1985).

25. He, P. *et al.* A human fetal lung cell atlas uncovers proximal-distal gradients of differentiation and key regulators of epithelial fates. *Cell* **185**, 4841-4860.e25 (2022).
26. Lim, K. *et al.* Organoid modeling of human fetal lung alveolar development reveals mechanisms of cell fate patterning and neonatal respiratory disease. *Cell Stem Cell* **30**, 20-37.e9 (2023).
27. Inman, G. J. *et al.* SB-431542 is a potent and specific inhibitor of transforming growth factor-beta superfamily type I activin receptor-like kinase (ALK) receptors ALK4, ALK5, and ALK7. *Mol Pharmacol* **62**, 65–74 (2002).
28. Laping, N. J. *et al.* Inhibition of transforming growth factor (TGF)-beta1-induced extracellular matrix with a novel inhibitor of the TGF-beta type I receptor kinase activity: SB-431542. *Mol Pharmacol* **62**, 58–64 (2002).
29. Dobbs, L. G., Gonzalez, R. F., Allen, L. & Froh, D. K. HTI56, an integral membrane protein specific to human alveolar type I cells. *J Histochem Cytochem* **47**, 129–137 (1999).
30. Liu, Z. *et al.* MAPK-Mediated YAP Activation Controls Mechanical-Tension-Induced Pulmonary Alveolar Regeneration. *Cell Rep* **16**, 1810–1819 (2016).
31. Wu, H. *et al.* Progressive Pulmonary Fibrosis Is Caused by Elevated Mechanical Tension on Alveolar Stem Cells. *Cell* **180**, 107-121.e17 (2020).
32. Chung, M.-I., Bujnis, M., Barkauskas, C. E., Kobayashi, Y. & Hogan, B. L. M. Niche-mediated BMP/SMAD signaling regulates lung alveolar stem cell proliferation and differentiation. *Development* **145**, dev163014 (2018).
33. Horani, A., Nath, A., Wasserman, M. G., Huang, T. & Brody, S. L. Rho-associated protein kinase inhibition enhances airway epithelial Basal-cell proliferation and lentivirus transduction. *Am J Respir Cell Mol Biol* **49**, 341–347 (2013).
34. Sikkema, L. *et al.* An integrated cell atlas of the lung in health and disease. *Nat Med* **29**, 1563–1577 (2023).

35. Nantie, L. B. *et al.* Lats1/2 inactivation reveals Hippo function in alveolar type I cell differentiation during lung transition to air breathing. *Development* **145**, dev163105 (2018).
36. DiGiovanni, G. T. *et al.* Epithelial Yap/Taz are required for functional alveolar regeneration following acute lung injury. *JCI Insight* e173374 (2023) doi:10.1172/jci.insight.173374.
37. LaCanna, R. *et al.* Yap/Taz regulate alveolar regeneration and resolution of lung inflammation. *J Clin Invest* **129**, 2107–2122 (2019).
38. Szklarczyk, D. *et al.* The STRING database in 2023: protein-protein association networks and functional enrichment analyses for any sequenced genome of interest. *Nucleic Acids Res* **51**, D638–D646 (2023).
39. Jang, J.-W., Kim, M.-K. & Bae, S.-C. Reciprocal regulation of YAP/TAZ by the Hippo pathway and the Small GTPase pathway. *Small GTPases* **11**, 280–288 (2020).
40. Pichaud, F., Walther, R. F. & Nunes de Almeida, F. Regulation of Cdc42 and its effectors in epithelial morphogenesis. *J Cell Sci* **132**, jcs217869 (2019).
41. Katzen, J. & Beers, M. F. Contributions of alveolar epithelial cell quality control to pulmonary fibrosis. *J Clin Invest* **130**, 5088–5099 (2020).
42. Li, W. *et al.* New insights into the pathogenesis of Hermansky-Pudlak syndrome. *Pigment Cell Melanoma Res* **35**, 290–302 (2022).
43. Vicary, G. W., Vergne, Y., Santiago-Cornier, A., Young, L. R. & Roman, J. Pulmonary Fibrosis in Hermansky-Pudlak Syndrome. *Ann Am Thorac Soc* **13**, 1839–1846 (2016).
44. Strikoudis, A. *et al.* Modeling of Fibrotic Lung Disease Using 3D Organoids Derived from Human Pluripotent Stem Cells. *Cell Rep* **27**, 3709-3723.e5 (2019).
45. Perkins, T. N. & Oury, T. D. The perplexing role of RAGE in pulmonary fibrosis: causality or casualty? *Ther Adv Respir Dis* **15**, 17534666211016071 (2021).
46. Alder, J. K. & Armanios, M. Telomere-mediated lung disease. *Physiol Rev* **102**, 1703–1720 (2022).

47. Tan, Y. & Cahan, P. SingleCellNet: A Computational Tool to Classify Single Cell RNA-Seq Data Across Platforms and Across Species. *Cell Syst* **9**, 207-213.e2 (2019).

Figure legends

Figure 1. ScRNA-seq analysis of iRAPs. a. Schematic of the anatomical arrangement and markers of RAPs *in vivo*, based on ref. 14. **b.** Schematic of experimental design to generate iRAPs from LOs**. c.** Representative bright field images of iRAPs generated from ESCs. **d.** iRAPs generated from mixed LO single cells expressing either GFP or mScarlet. **e.** Feature plots for indicated markers. **f.** Cell identity assignment based on data from ref. 14. **g.** scVelo latent time velocity analysis. **h.** Cell identity assignment based on data of ref. 12 with inclusion of data from IPF lungs.

Figure 2. Characterization if iRAPs. a. mRNA expression of indicated markers in iRAPs compared to LOs. ****p<0.0001, two-way ANOVA with Sidak multiple comparison test, n=6. **b.** Representative confocal images after staining for indicated markers in iRAPs. Scale bar = 50 µm. **c.** Representative WB for processed SFTPB and SFTPC in ESCs, in two ESC-derived iRAP lines, and in human adult lung. **d.** Representative flow cytometry plot for HT2-280 in iRAPs (left) with quantification (right). **p<0.01, student's unpaired t-test, n=3. **e.** Transmission electron microscopy of ESC-derived iRAPs (i = 40x, ii = 2000x, and iii = 4000x, arrows: LBs).

Figure 3. **Generation of D-iRAPs. a.** Schematic of experimental design. **b.** Representative bright field image of D-iRAPs. Scale bar = 200 µm. **c.** Representative flow cytometry histograms (left) and the quantification (right) of expression of HT1-56 and HT2-280 in indicated conditions. *p<0.05, **p<0.01, ***p<0.001, ****p<0.0001, one-way ANOVA with Tukey multiple comparison test, n=3. **d.** Expression of mRNA for the indicated markers in iRAPs and D-iRAPs. **** p<0.0001 two-way ANOVA with Sidak multiple comparison test, n=3. **e.** Z-stack projection of representative 3D confocal images after staining indicated markers. Scale bars = 100 µm. **f.** Quantification of (**e**) in D-iRAPs (pooled from 4 independent replicates). **g.** Cell identity assignment in D-iRAP scRNA-seq dataset based on markers shown in **(h)**. **h.** UMAP feature plots of indicated markers.

Figure 4. Generation of iAT1 cells. a. Schematic of experimental design. **b.** mRNA expression for the indicated markers in various conditions. *p<0.05, ****p<0.0001 One-way ANOVA with Tukey multiple comparison test, n≥4. **c.** Representative confocal images after staining for indicated markers in ALI supported by SB-BMP (iAT1) or DCI-SB (CTRL). Scale bars = 50 µm. **d.** Quantification of (**c**). *p<0.05, Student's unpaired t-test, n≥3. **e**. Representative flow cytometry plot for HT1-56 (left) and quantification for HT1-56 and HT2-280 (right), n=3. **f.** Cell identity assignment based on Human Lung Cell Atlas of iAT1 scRNA-seq dataset (top left) with UMAP feature plots of indicated markers.

Figure 5. Transcriptomic analysis of iAT1 generation. a. Schematic of experimental design. **b.** UMAP of merged analysis of scRNA-seq of iRAPs, D-iRAPs and iAT1 cells. **c.** UMAP feature plots of indicated markers. **d.** Dot plot showing expression of indicated markers in scRNAseq of of iRAPs, D-iRAPs and iAT1 cells. **e.** Heat map of differentially expressed distal lung-associated genes from RNAseq of iRAPs, D-iRAPs and iAT1 cells. Data represent normalized counts. **f.** Expression of the indicated genes in RNAseq of iRAPs, D-iRAPs and iAT1 cells. **g.** AT1-related differentially enriched GO pathways. **h.** Heat map of expression of genes associated with Hippo signaling. Data represent normalized counts. **i.** Interaction map of differentially expressed genes belonging to actomyosin, Hippo and tight junction assembly GO pathways generated using STRING-DB.

Figure 6. Phenotypes of *HSP1*$^{-/-}$ iRAPs. a. Differentiation schematic (iRAP highlighted). **b.** UMAP feature plots of indicated markers in *WT* and *HPS1*$^{-/-}$ iRAPs **c.** mRNA expression for indicated markers in *WT* and *HPS1*$^{-/-}$ iRAPs. *p<0.05, **p<0.01, Student's unpaired t-test, *WT* n=6, *HPS1*$^{-/-}$ n=3. **d.** Representative images of Lysotracker® uptake in iRAPs (left Scale bar = 250 µm), with flow cytometric quantification (right). ***p<0.001, One-way ANOVA with Dunnett's multiple comparison test, n=3. **e,f.** mRNA expression for indicated markers after 5 hours of 5 ng/mL tunicamycin exposure. *p<0.05, **p<0.01, Student's unpaired t-test, n=3. **g.** Apoptosis

after 5 days of 0.1 mg/mL tunicamycin treatment normalized to untreated iRAPs of the same genotype. *p<0.05, Student's unpaired t-test, n≥4. **h**. Differentiation schematic (D-iRAP highlighted) **i.** Representative flow cytometry plot for HT1-56 (left) with quantification of HT1-56^{+} cells in *HSP1*$^{-/-}$ D-iRAPs normalized to *WT* (right). **p<.01, Student's unpaired t-test, n=11. **j.** mRNA expression for *AGER* mRNA in *HPS1*$^{-/-}$ and *WT* D-iRAPs. **p<0.01, Student's t-test, n=3. **k.** Differentiation schematic (iAT1 highlighted) **l.** Representative flow cytometry histogram of HT1-56 staining intensity (left) with quantification (right) in *WT* and *HSP1*$^{-/-}$ iAT1 cells. *p<0.05, Student's unpaired t-test, n=9. **m.** mRNA expression for *AGER* mRNA in *HPS1*$^{-/-}$ and *WT* iAT1 cells. Student's t-test, n=3.

Fig. 1

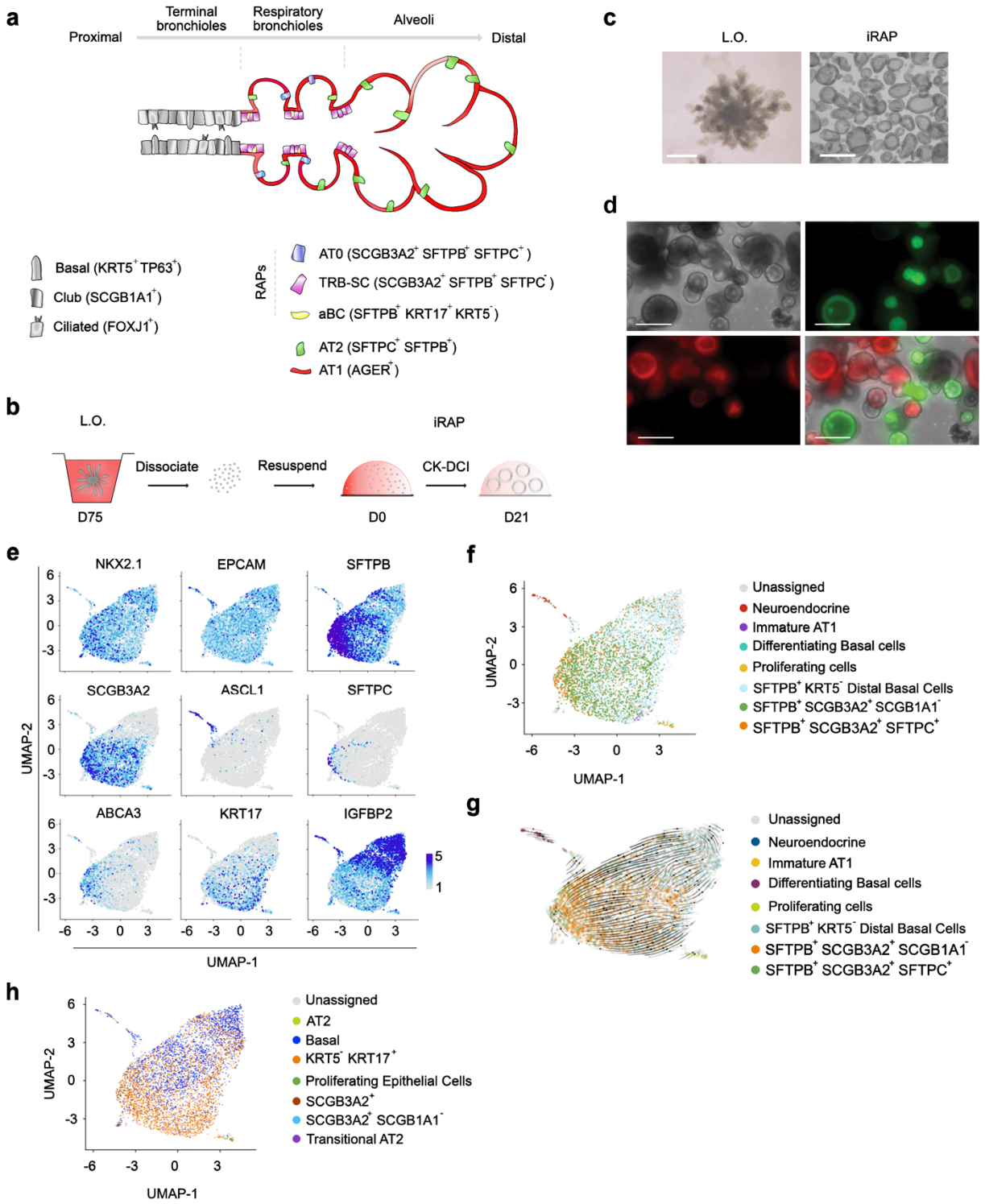
a
Proximal
Terminal bronchioles
Respiratory bronchioles
Alveoli
Distal
Basal (KRT5+ TP63+)
Club (SCGB1A1+)
Ciliated (FOXJ1+)
RAPs
AT0 (SCGB3A2+ SFTPB+ SFTPC+)
TRB-SC (SCGB3A2+ SFTPB+ SFTPC-)
aBC (SFTPB+ KRT17+ KRT5-)
AT2 (SFTPC+ SFTPB+)
AT1 (AGER+)
b
L.O.
iRAP
Dissociate
Resuspend
CK-DCI
D75
D0
D21
c
L.O.
iRAP
d
e
NKX2.1
EPCAM
SFTPB
SCGB3A2
ASCL1
SFTPC
ABCA3
KRT17
IGFBP2
UMAP-2
UMAP-1
f
Unassigned
Neuroendocrine
Immature AT1
Differentiating Basal cells
Proliferating cells
SFTPB+ KRT5- Distal Basal Cells
SFTPB+ SCGB3A2+ SCGB1A1-
SFTPB+ SCGB3A2+ SFTPC+
UMAP-2
UMAP-1
g
Unassigned
Neuroendocrine
Immature AT1
Differentiating Basal cells
Proliferating cells
SFTPB+ KRT5- Distal Basal Cells
SFTPB+ SCGB3A2+ SCGB1A1-
SFTPB+ SCGB3A2+ SFTPC+
h
Unassigned
AT2
Basal
KRT5- KRT17+
Proliferating Epithelial Cells
SCGB3A2+
SCGB3A2+ SCGB1A1-
Transitional AT2
UMAP-2
UMAP-1

Fig. 2

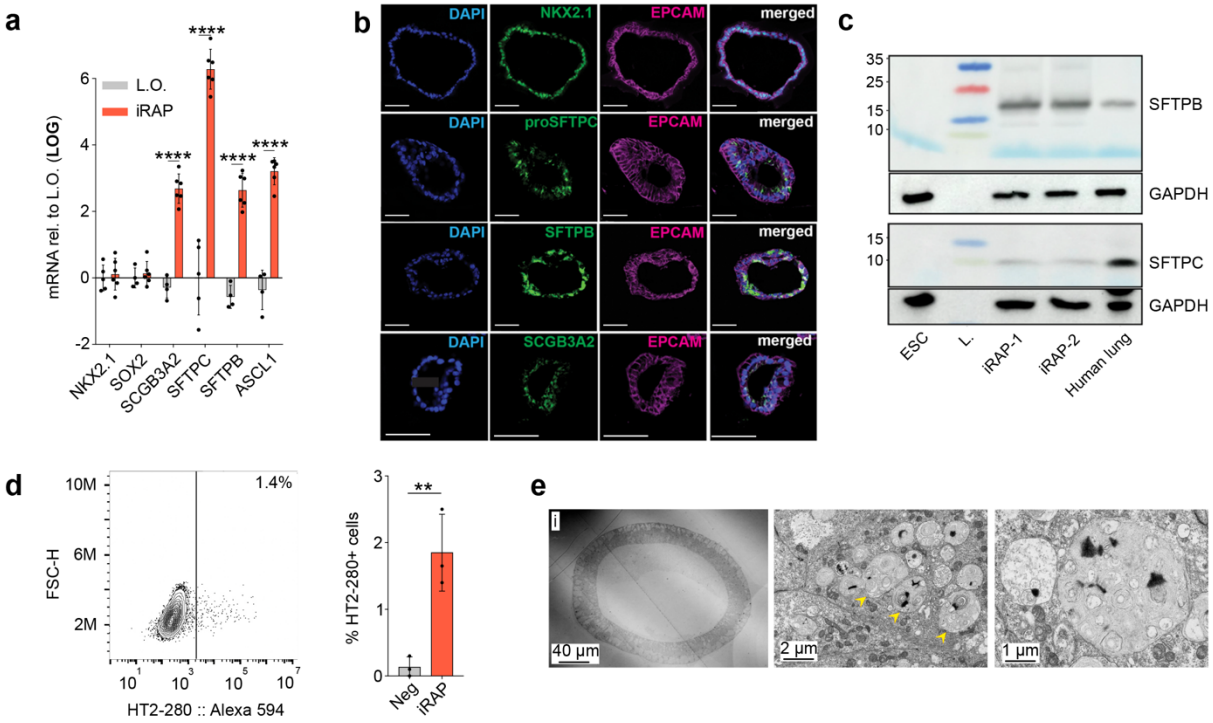
a
L.O.
iRAP
mRNA rel. to L.O. (LOG)
****
NKX2.1
SOX2
SCGB3A2
SFTPC
SFTPB
ASCL1
b
DAPI
NKX2.1
EPCAM
merged
proSFTPC
SFTPB
SCGB3A2
c
SFTPB
GAPDH
SFTPC
ESC
L.
iRAP-1
iRAP-2
Human lung
d
1.4%
FSC-H
HT2-280 :: Alexa 594
% HT2-280+ cells
**
Neg
iRAP
e
40 µm
2 µm
1 µm

Fig. 3

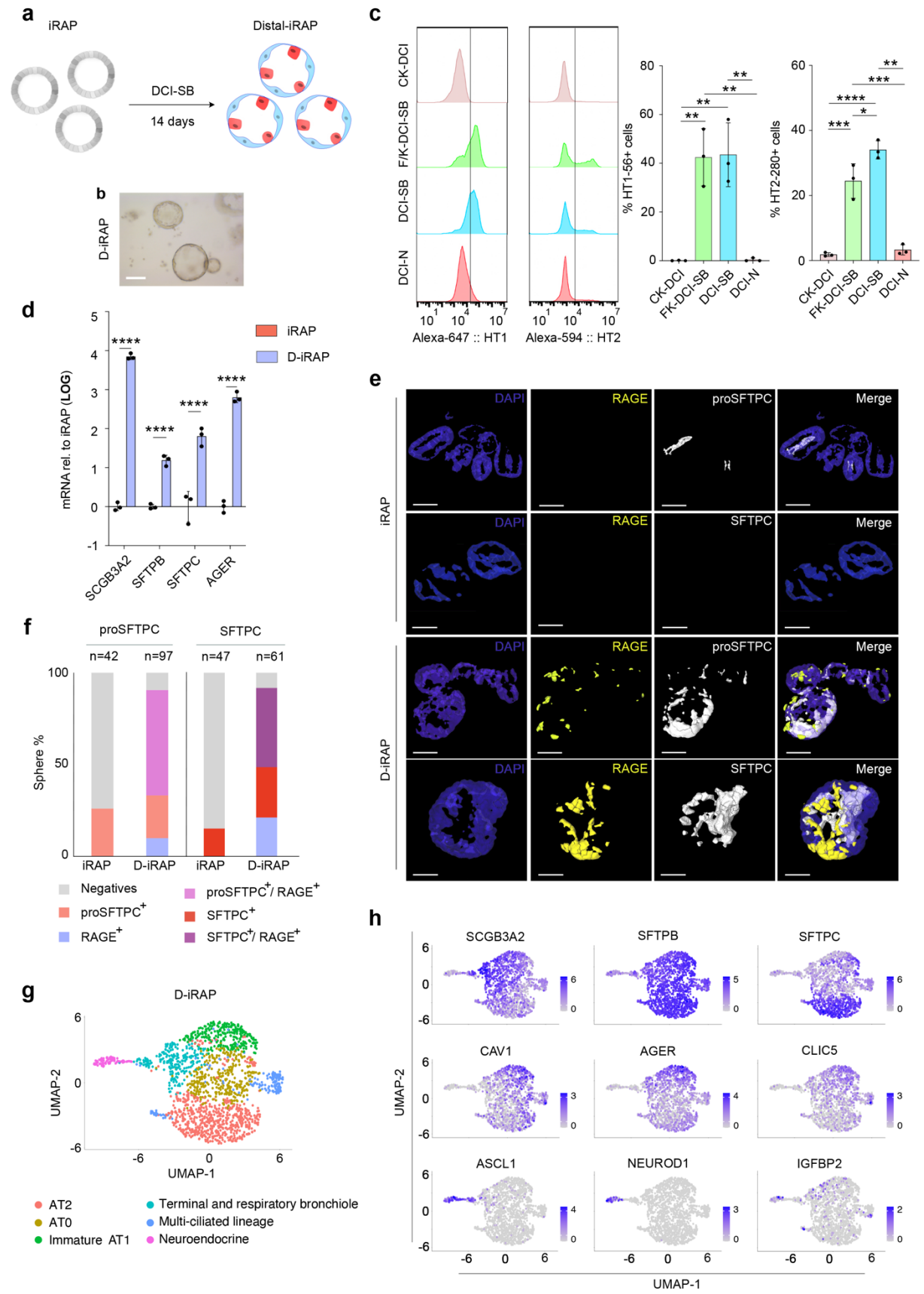
a
iRAP
Distal-iRAP
DCI-SB
14 days
b
D-iRAP
c
CK-DCI
F/K-DCI-SB
DCI-SB
DCI-N
Alexa-647 :: HT1
Alexa-594 :: HT2
% HT1-56+ cells
% HT2-280+ cells
d
iRAP
D-iRAP
mRNA rel. to iRAP (LOG)
SCGB3A2
SFTPB
SFTPC
AGER
e
DAPI
RAGE
proSFTPC
SFTPC
Merge
iRAP
D-iRAP
f
proSFTPC
SFTPC
n=42
n=97
n=47
n=61
Sphere %
iRAP
D-iRAP
Negatives
proSFTPC+
RAGE+
proSFTPC+/ RAGE+
SFTPC+
SFTPC+/ RAGE+
g
D-iRAP
UMAP-2
UMAP-1
AT2
AT0
Immature AT1
Terminal and respiratory bronchiole
Multi-ciliated lineage
Neuroendocrine
h
SCGB3A2
SFTPB
SFTPC
CAV1
AGER
CLIC5
ASCL1
NEUROD1
IGFBP2
UMAP-2
UMAP-1

Fig. 4

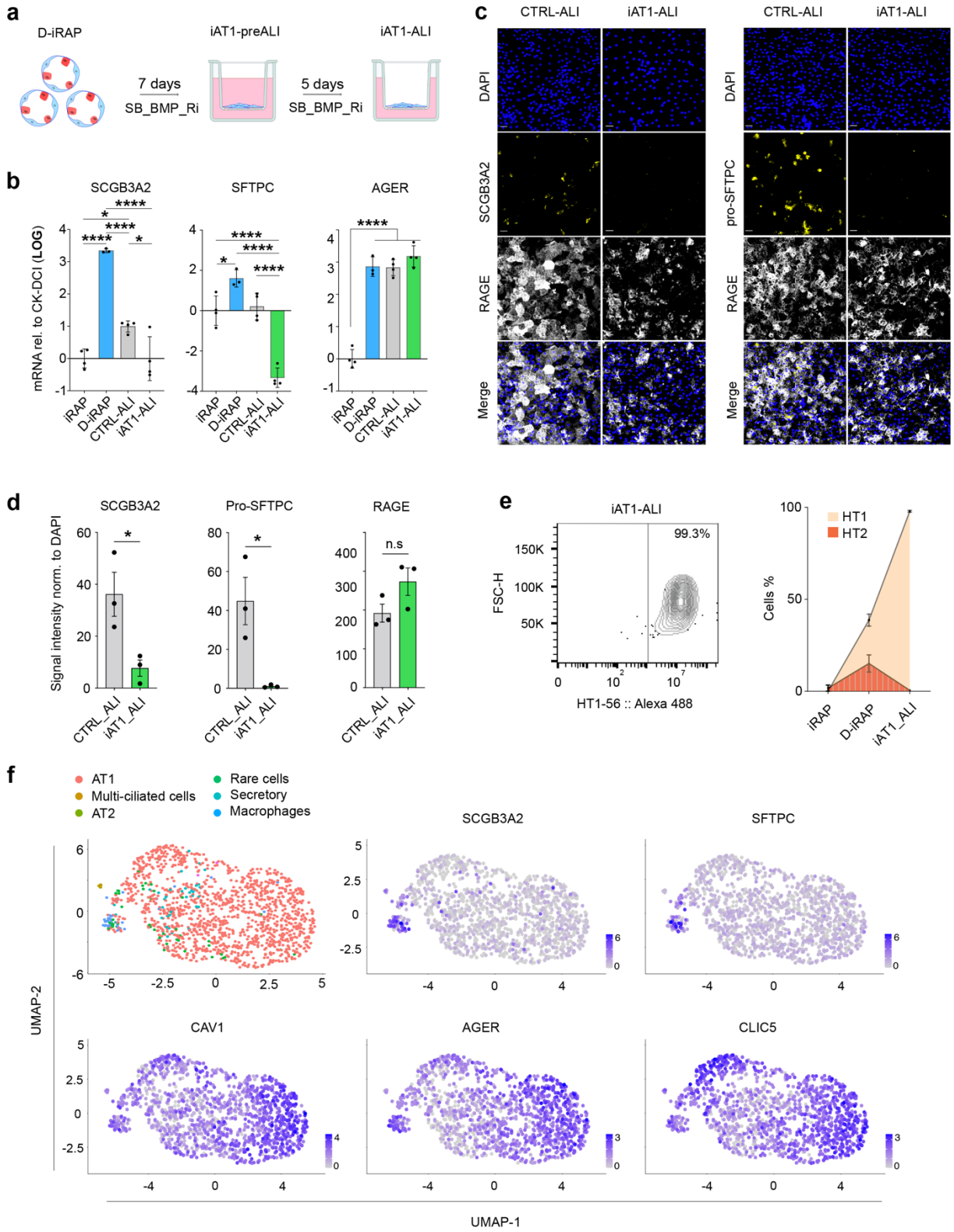
a
D-iRAP
iAT1-preALI
iAT1-ALI
7 days
SB_BMP_Ri
5 days
SB_BMP_Ri
b
SCGB3A2
SFTPC
AGER
mRNA rel. to CK-DCI (LOG)
iRAP
D-iRAP
CTRL-ALI
iAT1-ALI
c
CTRL-ALI
iAT1-ALI
DAPI
SCGB3A2
pro-SFTPC
RAGE
Merge
d
SCGB3A2
Pro-SFTPC
RAGE
Signal intensity norm. to DAPI
n.s
CTRL_ALI
iAT1_ALI
e
iAT1-ALI
99.3%
FSC-H
HT1-56 :: Alexa 488
HT1
HT2
Cells %
iRAP
D-iRAP
iAT1_ALI
f
AT1
Multi-ciliated cells
AT2
Rare cells
Secretory
Macrophages
SCGB3A2
SFTPC
CAV1
AGER
CLIC5
UMAP-2
UMAP-1

Fig. 5

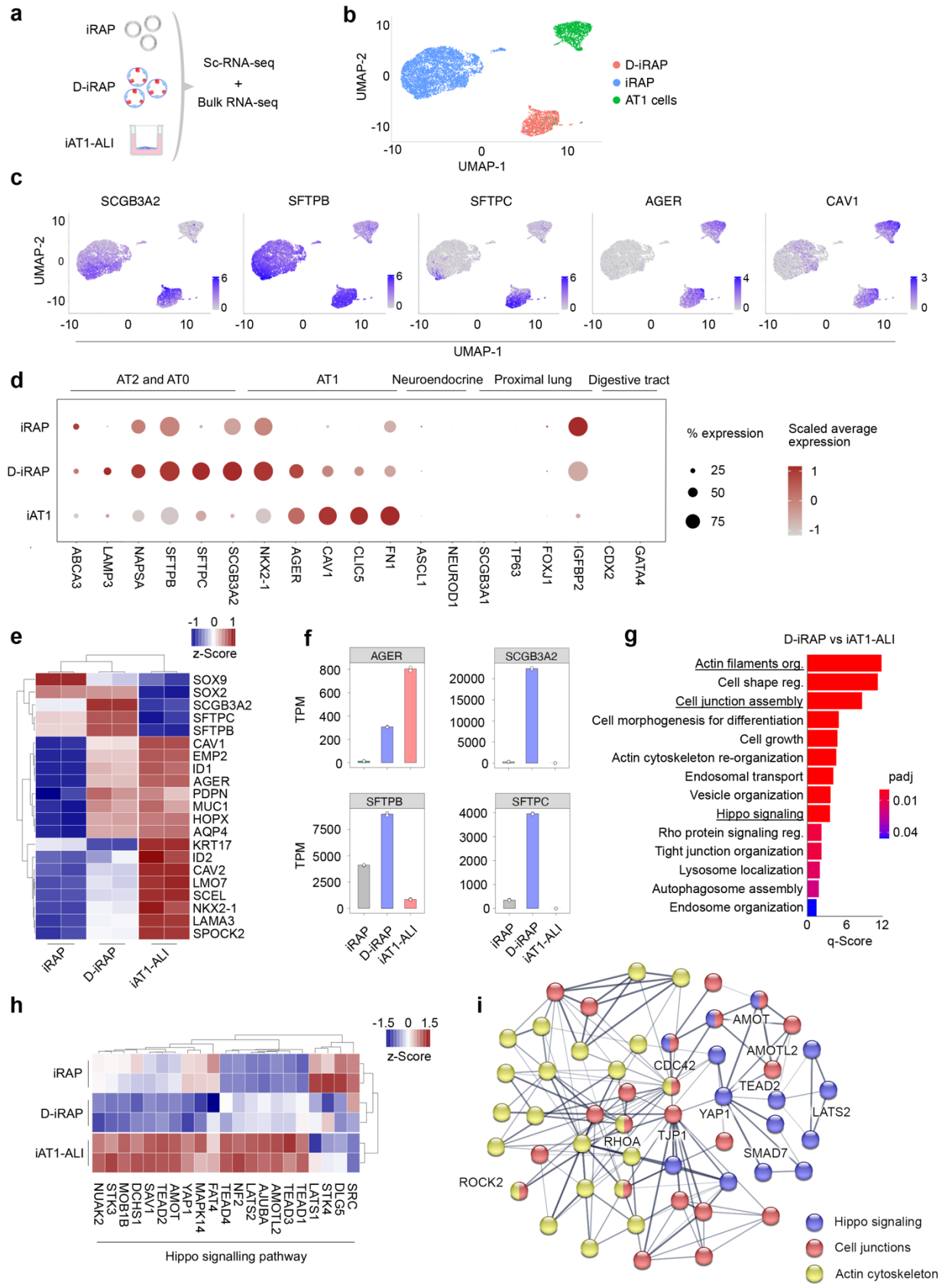
a
iRAP
D-iRAP
iAT1-ALI
Sc-RNA-seq
+
Bulk RNA-seq
b
UMAP-2
UMAP-1
D-iRAP
iRAP
AT1 cells
c
SCGB3A2
SFTPB
SFTPC
AGER
CAV1
UMAP-2
UMAP-1
d
AT2 and AT0
AT1
Neuroendocrine
Proximal lung
Digestive tract
iRAP
D-iRAP
iAT1
ABCA3
LAMP3
NAPSA
SFTPB
SFTPC
SCGB3A2
NKX2-1
AGER
CAV1
CLIC5
FN1
ASCL1
NEUROD1
SCGB3A1
TP63
FOXJ1
IGFBP2
CDX2
GATA4
% expression
25
50
75
Scaled average expression
1
0
-1
e
z-Score
SOX9
SOX2
SCGB3A2
SFTPC
SFTPB
CAV1
EMP2
ID1
AGER
PDPN
MUC1
HOPX
AQP4
KRT17
ID2
CAV2
LMO7
SCEL
NKX2-1
LAMA3
SPOCK2
iRAP
D-iRAP
iAT1-ALI
f
AGER
SCGB3A2
SFTPB
SFTPC
TPM
iRAP
D-iRAP
iAT1-ALI
g
D-iRAP vs iAT1-ALI
Actin filaments org.
Cell shape reg.
Cell junction assembly
Cell morphogenesis for differentiation
Cell growth
Actin cytoskeleton re-organization
Endosomal transport
Vesicle organization
Hippo signaling
Rho protein signaling reg.
Tight junction organization
Lysosome localization
Autophagosome assembly
Endosome organization
padj
0.01
0.04
q-Score
h
z-Score
iRAP
D-iRAP
iAT1-ALI
NUAK2
STK3
MOB1B
DCHS1
SAV1
TEAD2
AMOT
YAP1
MAPK14
FAT4
TEAD4
NF2
LATS2
AJUBA
AMOTL2
TEAD3
TEAD1
LATS1
STK4
DLG5
SRC
Hippo signalling pathway
i
AMOT
AMOTL2
CDC42
TEAD2
YAP1
LATS2
RHOA
TJP1
SMAD7
ROCK2
Hippo signaling
Cell junctions
Actin cytoskeleton

Fig. 6

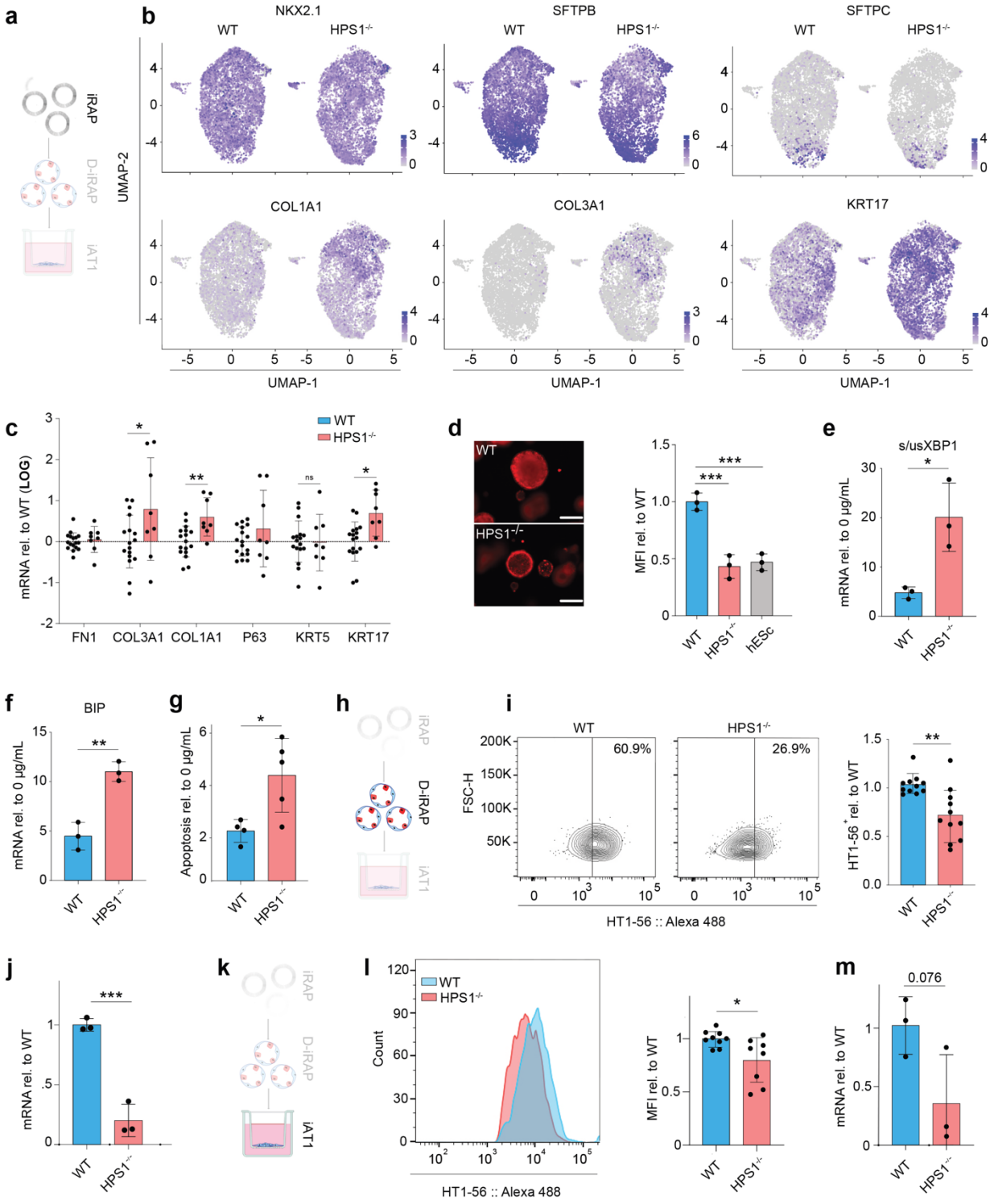
a
iRAP
D-iRAP
iAT1
b
NKX2.1
SFTPB
SFTPC
WT
HPS1-/-
UMAP-2
UMAP-1
COL1A1
COL3A1
KRT17
c
WT
HPS1-/-
mRNA rel. to WT (LOG)
FN1
COL3A1
COL1A1
P63
KRT5
KRT17
ns
d
WT
HPS1-/-
MFI rel. to WT
hESc
e
s/usXBP1
mRNA rel. to 0 µg/mL
f
BIP
mRNA rel. to 0 µg/mL
g
Apoptosis rel. to 0 µg/mL
h
i
FSC-H
60.9%
26.9%
HT1-56 :: Alexa 488
HT1-56+ rel. to WT
j
mRNA rel. to WT
k
l
Count
HT1-56 :: Alexa 488
MFI rel. to WT
m
0.076

Extended Data

ED1. iPSC-derived iRAPs. a. Representative bright-field image of iPS-derived iRAPs (scale bar = 400 μm). **b.** Representative expansion of iPSC-derived iRAPs (n=1). **c.** mRNA expression for indicated markers in iPSC-derived iRAPs compared to LOs. ** $p<0.01$, **** $p<0.0001$ two-way ANOVA with Sidak test for multiple comparisons, n=2. **d-e.** Representative confocal images for indicated markers of iRAPs generated from iPSCs. Scale bar = 50 μm. **f.** Representative WB for mature SFTPB and SFTPC in iPSC- and ESC-derived iRAPs and human adult lung. **g.** Representative flow cytometry plot for HT2-280. **h.** Representative bright-field image of iPS-derived D-iRAPs. Scale bar = 200 μm. **i.** Representative flow cytometry plot of iPS-derived D-iRAPs for HT2-280 (left) with quantification (right). Student's t-test, n=2). **j.** Representative flow cytometry plot for iPS-derived D-iRAPs HT1-56 (left) with quantification (right). *$p<0.05$, Student's t-test, n=3.

ED2. Further characterization of iRAPs. a. Expansion of ESC-derived iRAPs (n=3). **b.** Representative confocal image for selected markers. Scale bar = 50 μm **c.** Representative image of Lysotracker Red uptake. Scale bar = 200 μm **d.** Expression mRNA for indicated genes at consecutive passages relative to LOs. **e.** mRNA expression for lung-specific markers in ESC-derived iRAPs derived from day 120 relative to from d42 LOs. Two-way ANOVA with Sidak's multiple comparison test (n=3). **f.** mRNA expression for lung-specific markers in ESC-derived iRAPs after cryopreservation relative to fresh iRAPs. Two-way ANOVA with Sidak's multiple comparison test (n=3).

ED3. Gating strategy. Representative example of live cells gating and doublet exclusion used throughout this report.

ED4. Establishment of conditions to induce D-iRAPs. a. Representative bright field images after CHIR withdrawal. Scale bar = 200 μm. **b.** Representative IF for indicated markers. Scale bars = 100 μm. **c.** Representative flow cytometry plot (left) with quantification of HT2-280^{+} cells

(right). **** p<0.0001, Student's t-test, n=3. **d.** mRNA expression for indicated markers after CHIR withdrawal. ***p<0.001, two-way ANOVA with Sidak multiple comparison test (n=3). **e.** RT-qPCR for after addition of DAPT. *** p<0.001, Two-way ANOVA with Sidak multiple comparison test (n=3). **f.** Representative flow cytometry plot (left) with quantification (right) of HT2-280$^+$ cells. Student's t-test, n=3.

ED5. Signaling pathways involved in human AT1 and AT2 development. a. Cluster analysis of human embryonic lung sc-RNA-seq dataset. "Lung epithelium" cluster identity based on gene expression analysis in (**b**). **b.** UMAP feature plots for indicated markers. **c.** Cluster analysis after sub-setting 'Lung epithelium' cluster. Cluster identity based on gene expression in **(d)**. **d.** UMAP feature plots for indicated markers. **e.** Cell type analysis 100 top DEGs in "AT1-AT2 progenitor" cluster. **f.** GO term analysis (Panther) of 100 top DEGs in "AT1-AT2 progenitor" cluster. **g.** UMAP feature plots for indicated markers.

ED6. Further characterization of D-iRAPs. a-c. Representative flow cytometry plots for indicated markers and conditions. **d.** Quantification of flow cytometry shown in **(b)** and **(c)**. *p<0.05, **p<0.01, ****p<0.0001, one-way ANOVA with Tukey multiple comparison test (n=3). **e.** mRNA expression for indicated markers in conditions shown in X-axis. *p<0.05, **p<0.01, ***p<0.001, one-way ANOVA with Tukey multiple comparison test. **f & h.** Surface reconstitution based on indicated marker fluorescent intensity. Scale bar = 150 μm**.** **g.** 3D reconstitution of representative confocal 3D images for indicated markers. Scale bars = 50 μm. **i.** Fluorescent signal intensity quantification of the indicated markers. *p<0.05, ****p<0.0001, Student's t-test, n=42 iRAPs and n=97 D-iRAP spheres from 4 independent replicates. **j.** Cell viability during differentiation of D-iRAPs from iRAPs in DCI-SB conditions for up to 21 days, ***p<0.001, two-way ANOVA with multiple comparison using Sidak test, n=3.

ED7. Further characterization of iAT1 differentiation. a. Schematic of iAT1 differentiation in 2D submerged culture. **b.** Representative bright field images of 2D submerged cultures in the

indicated conditions. Scale bar = 200 µm. **c.** mRNA expression for indicated markers in conditions shown in the X-axis. *p<0.05, **p<0.01, ***p<0.001, ****p<0.0001, one-way ANOVA with Tukey multiple comparison test (n=3). **d.** Representative confocal images after staining for indicated markers in conditions shown on the left. Scale bars = 50 µm. **e**. Schematic of iAT1 differentiation in 2D ALI culture. **f.** Representative bright field image of ALI culture in SB-BMP. Scale bar = 200 µm. **g.** Representative confocal images after staining for indicated markers (left) with quantification (right). Scale bars = 50 µm. *p<0.05, Student's t-test, n=3. **h.** Representative confocal images showing SFTPB and AGER colocalization (left) with quantification (right). Scale bars = 100 µm. *p<0.05, Student's t-test, n=3.

ED8. Bulk RNA-seq of iAT1 differentiation a. Heat map representing normalized gene counts throughout iAT1 differentiation. **b.** Venn diagram showing the number of DEGs between the indicated samples. **c.** Top 10 up (red) and down (blue) regulated GO pathways between D-iRAPs and iAT1 cells . **d.** Idem between iRAPs and iAT1 cells. **e.** Protein-protein interaction analysis pipeline analysis.

ED9. Further characterization of *HSP1*$^{-/-}$ iRAPs a. mRNA expression for lung markers in *HPS1*$^{-/-}$ and WT iRAPs. Student's unpaired t-test, WT n=6, HPS1$^{-/-}$ n=3. **b.** Days per population doubling in WT and HPS1$^{-/-}$ iRAPs. *p<.05, Two-way ANOVA with Sidak's multiple comparison test, n≥3. **c.** Representative flow cytometry histogram of Lysotracker® uptake in WT and *HSP1*$^{-/-}$ iRAPs. **d.** Representative flow cytometry histogram of propidium iodide staining of iRAPs with and without 5 days of 0.1 ng/mL tunicamycin exposure. **e.** Representative flow cytometry contour plot of HT2-280 expression in WT and *HPS1*$^{-/-}$ D-iRAPs (left) with quantification of HT2-280^{+} cells in *HSP1*$^{-/-}$ D-iRAPs normalized to WT. *p<.05, Student's unpaired t-test, n≥10. **f.** mRNA expression for indicated markers in *WT* and *HPS1*$^{-/-}$ D-iRAPs compared to iRAPs of the same genotype. ***p<0.001, Two-way ANOVA with Tukey's multiple comparison, n=3. **g.** Representative flow

cytometry plots of HT1-56 and HT2-280 expression in *WT* and *HPS1*$^{-/-}$ iAT1 cells. **h.** Quantification of (**g**).

ED1

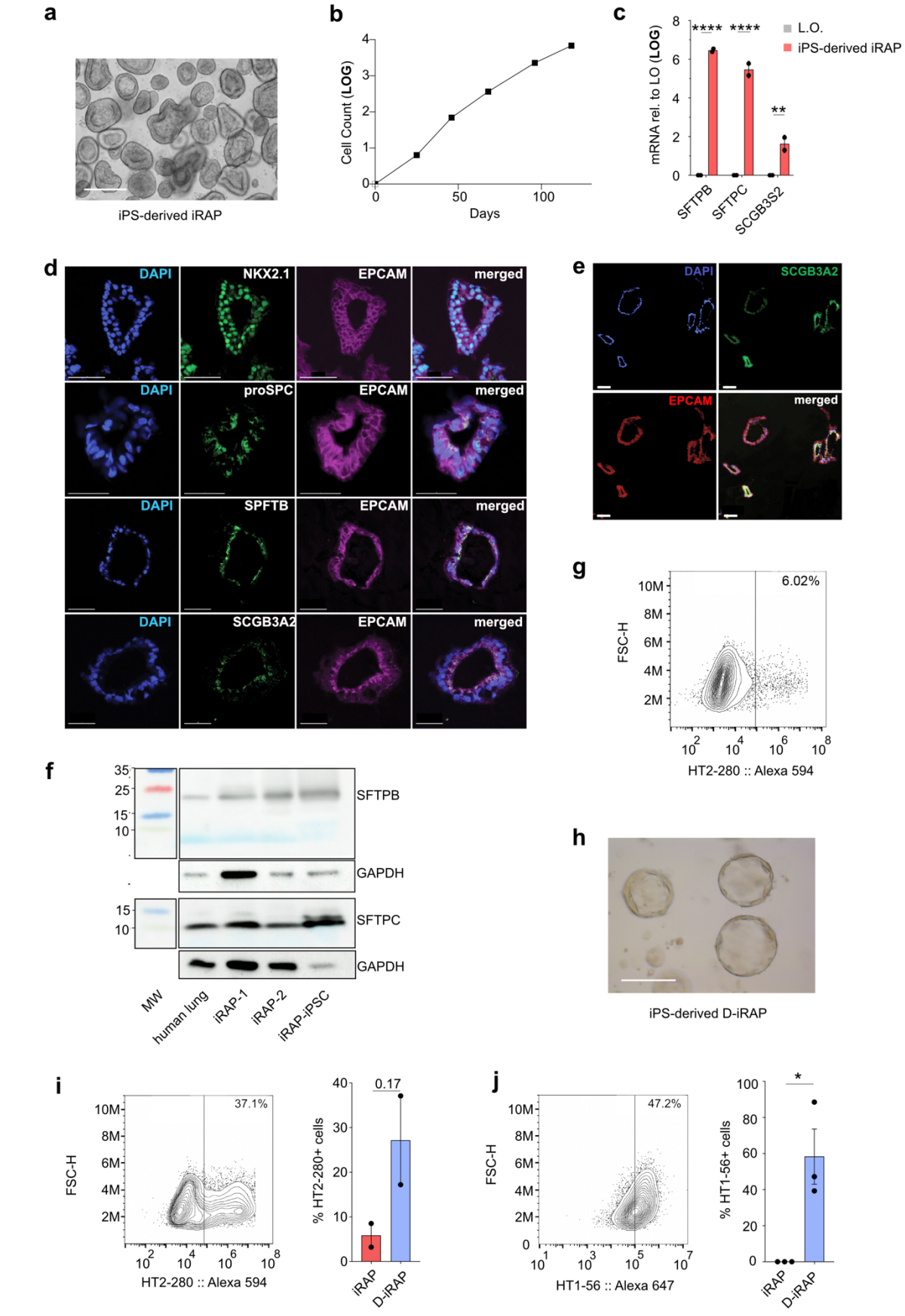

a
iPS-derived iRAP
b
Cell Count (LOG)
Days
c
mRNA rel. to LO (LOG)
L.O.
iPS-derived iRAP
****
****
**
SFTPB
SFTPC
SCGB3S2
d
DAPI
NKX2.1
EPCAM
merged
proSPC
SPFTB
SCGB3A2
e
DAPI
SCGB3A2
EPCAM
merged
f
SFTPB
GAPDH
SFTPC
GAPDH
MW
human lung
iRAP-1
iRAP-2
iRAP-iPSC
g
6.02%
FSC-H
HT2-280 :: Alexa 594
h
iPS-derived D-iRAP
i
37.1%
FSC-H
HT2-280 :: Alexa 594
0.17
% HT2-280+ cells
iRAP
D-iRAP
j
47.2%
FSC-H
HT1-56 :: Alexa 647
*
% HT1-56+ cells
iRAP
D-iRAP

ED2

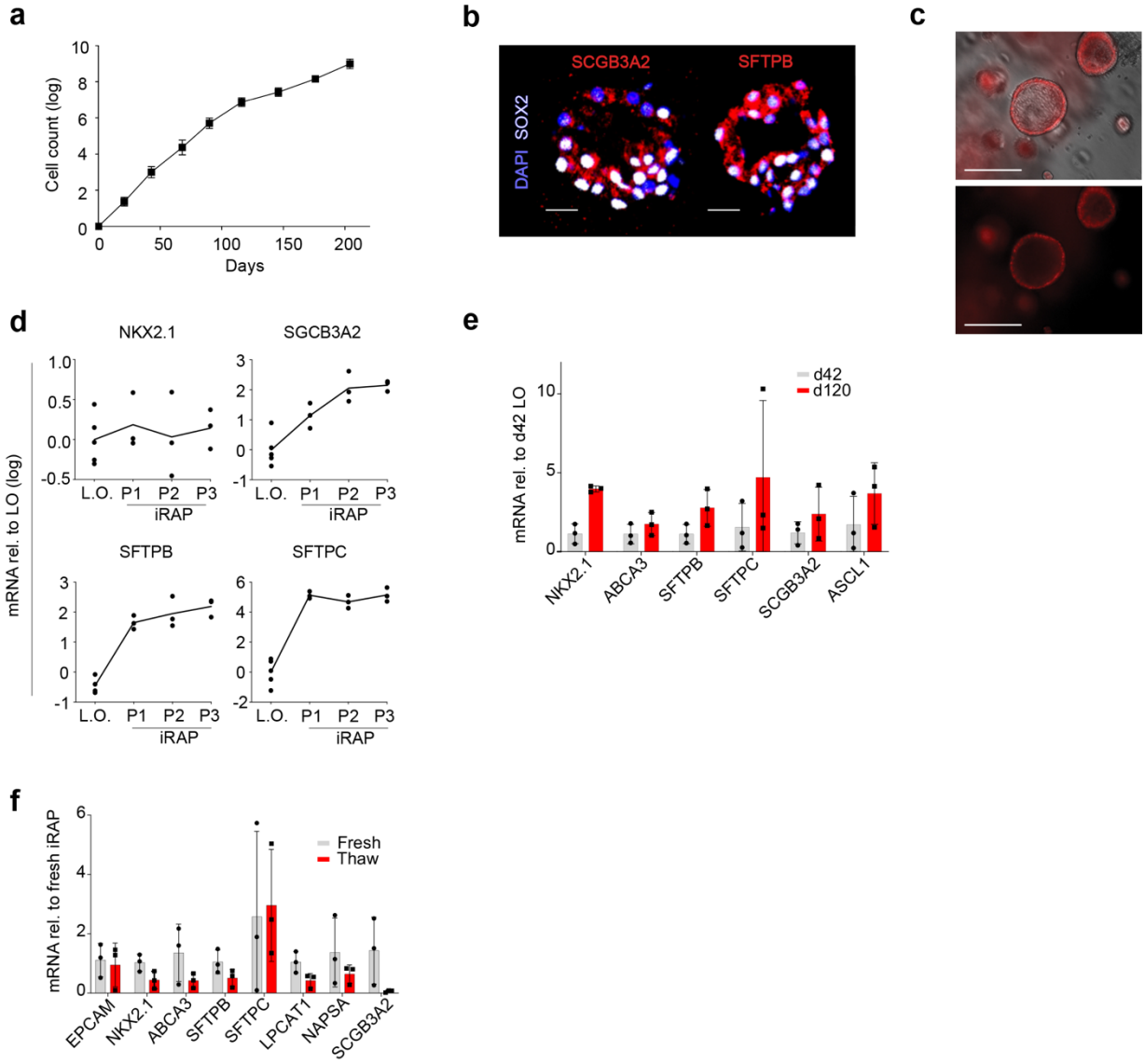
a
Cell count (log)
Days
b
SCGB3A2
SFTPB
DAPI SOX2
c
d
NKX2.1
SGCB3A2
SFTPB
SFTPC
mRNA rel. to LO (log)
L.O. P1 P2 P3
iRAP
e
d42
d120
mRNA rel. to d42 LO
NKX2.1
ABCA3
SFTPB
SFTPC
SCGB3A2
ASCL1
f
Fresh
Thaw
mRNA rel. to fresh iRAP
EPCAM
NKX2.1
ABCA3
SFTPB
SFTPC
LPCAT1
NAPSA
SCGB3A2

ED3

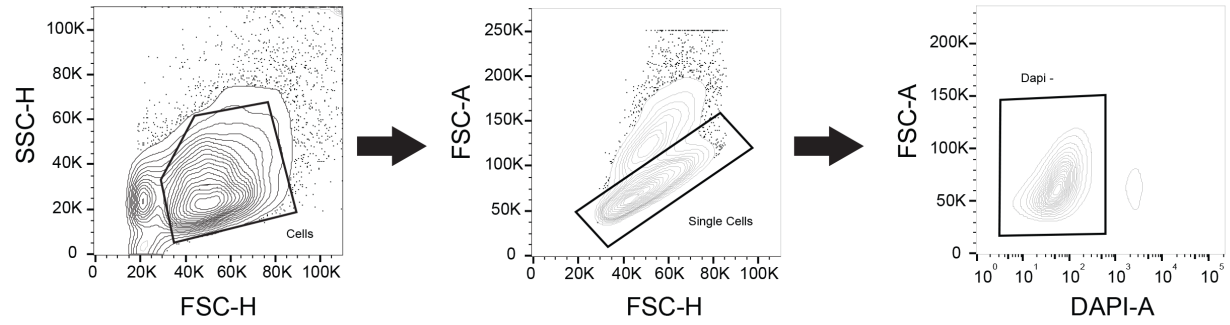

ED4

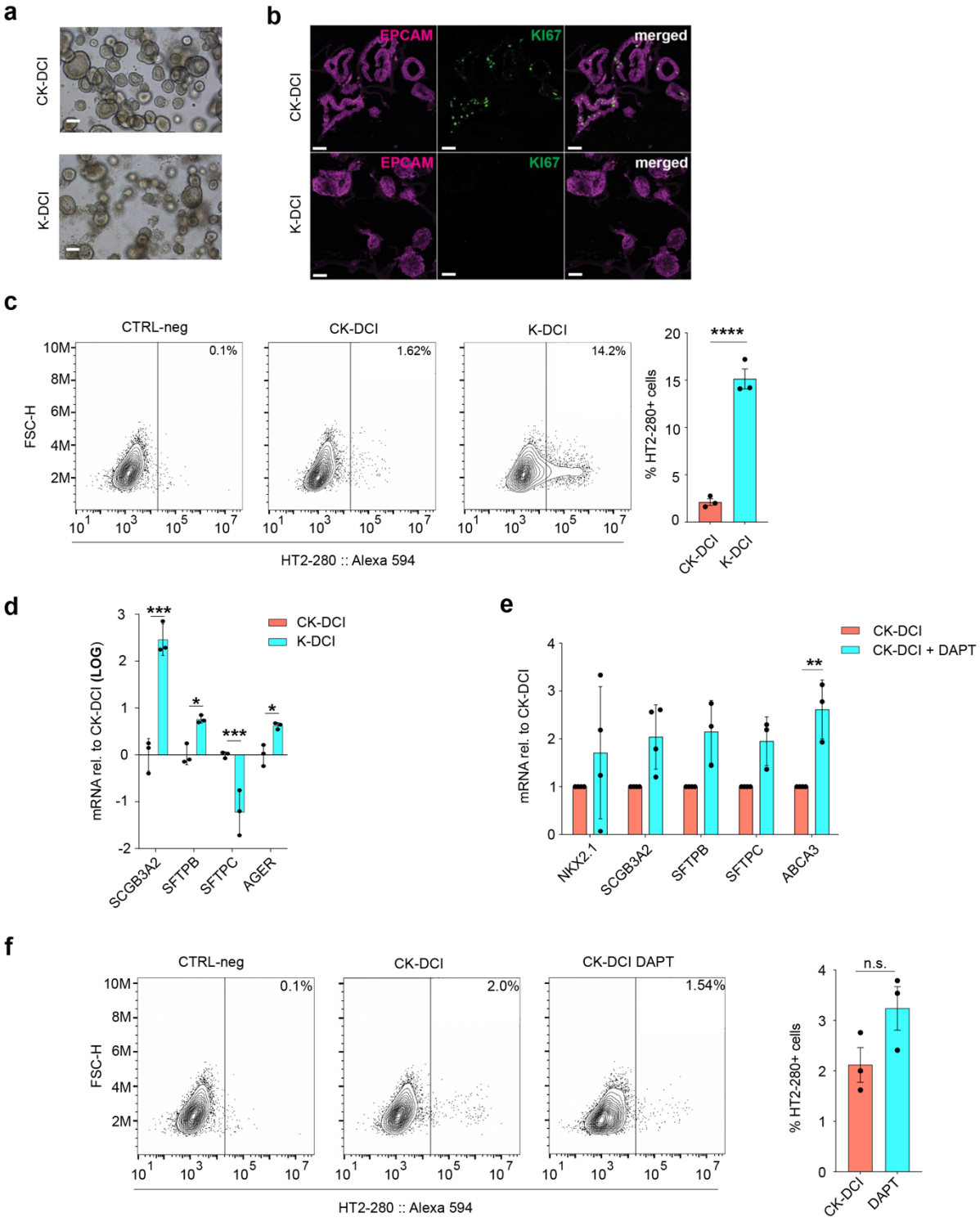
a
CK-DCI
K-DCI
b
EPCAM
KI67
merged
CK-DCI
K-DCI
c
CTRL-neg
CK-DCI
K-DCI
0.1%
1.62%
14.2%
FSC-H
10M
8M
6M
4M
2M
HT2-280 :: Alexa 594
% HT2-280+ cells
****
CK-DCI
K-DCI
d
mRNA rel. to CK-DCI (LOG)
CK-DCI
K-DCI
***
*
***
*
SCGB3A2
SFTPB
SFTPC
AGER
e
mRNA rel. to CK-DCI
CK-DCI
CK-DCI + DAPT
**
NKX2.1
SCGB3A2
SFTPB
SFTPC
ABCA3
f
CTRL-neg
CK-DCI
CK-DCI DAPT
0.1%
2.0%
1.54%
FSC-H
HT2-280 :: Alexa 594
% HT2-280+ cells
n.s.
CK-DCI
DAPT

ED5

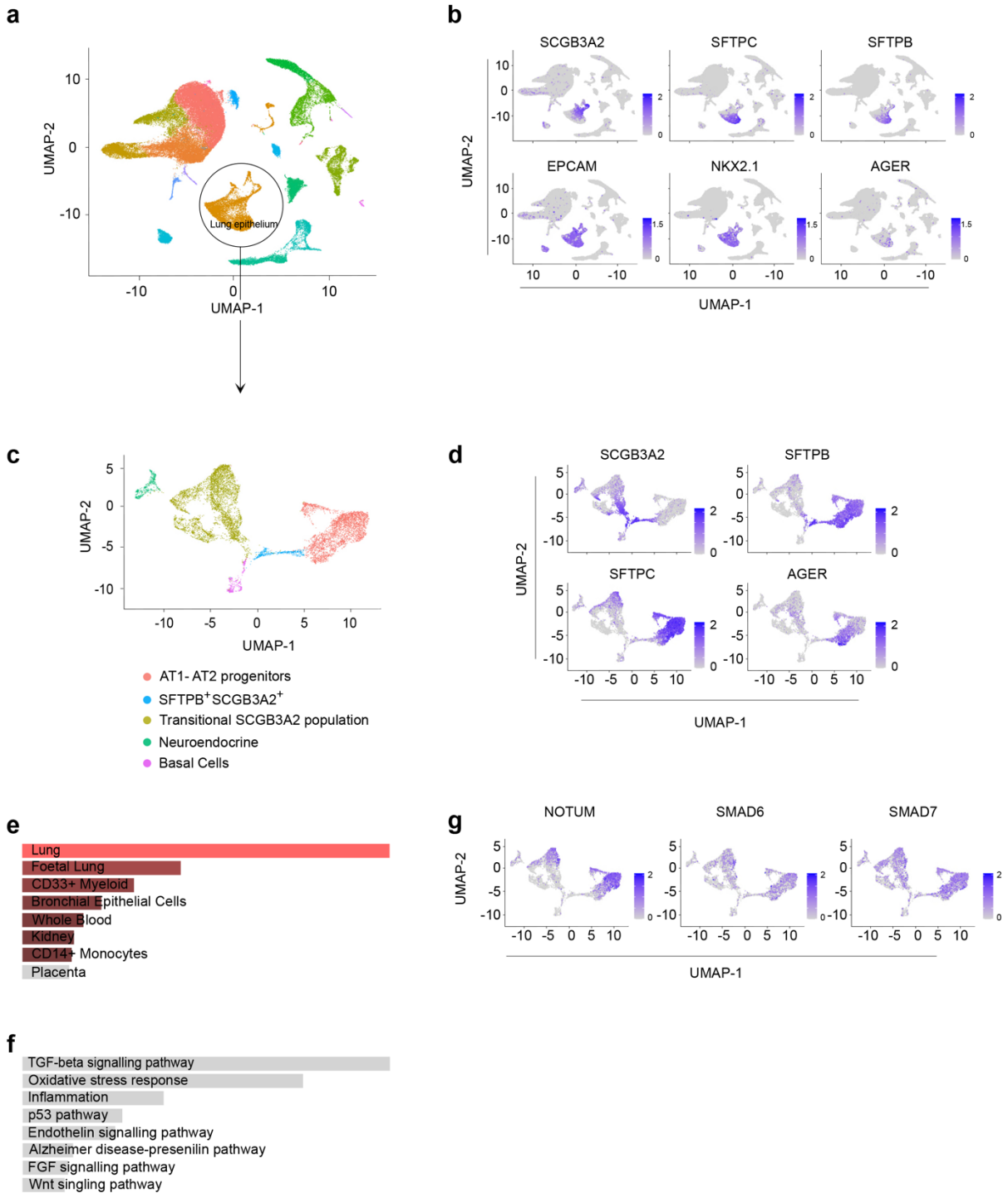
a
UMAP-2
UMAP-1
Lung epithelium
b
SCGB3A2
SFTPC
SFTPB
EPCAM
NKX2.1
AGER
UMAP-2
UMAP-1
c
UMAP-2
UMAP-1
AT1- AT2 progenitors
SFTPB+SCGB3A2+
Transitional SCGB3A2 population
Neuroendocrine
Basal Cells
d
SCGB3A2
SFTPB
SFTPC
AGER
UMAP-2
UMAP-1
e
Lung
Foetal Lung
CD33+ Myeloid
Bronchial Epithelial Cells
Whole Blood
Kidney
CD14+ Monocytes
Placenta
g
NOTUM
SMAD6
SMAD7
UMAP-2
UMAP-1
f
TGF-beta signalling pathway
Oxidative stress response
Inflammation
p53 pathway
Endothelin signalling pathway
Alzheimer disease-presenilin pathway
FGF signalling pathway
Wnt singling pathway

ED6

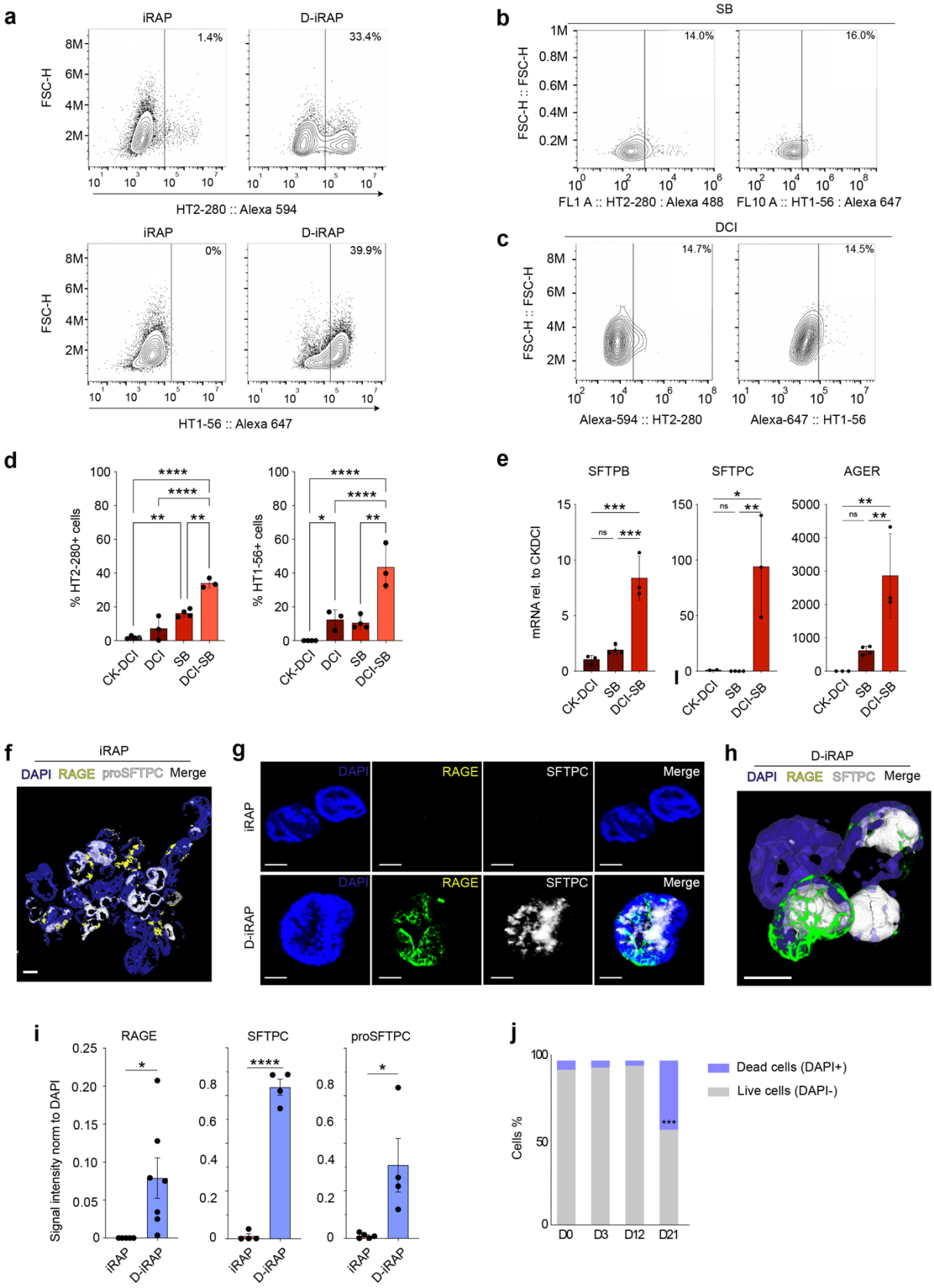
a
iRAP
D-iRAP
1.4%
33.4%
FSC-H
HT2-280 :: Alexa 594
0%
39.9%
HT1-56 :: Alexa 647
b
SB
14.0%
16.0%
FSC-H :: FSC-H
FL1 A :: HT2-280 : Alexa 488
FL10 A :: HT1-56 : Alexa 647
c
DCI
14.7%
14.5%
Alexa-594 :: HT2-280
Alexa-647 :: HT1-56
d
% HT2-280+ cells
% HT1-56+ cells
CK-DCI
DCI
SB
DCI-SB
e
SFTPB
SFTPC
AGER
mRNA rel. to CKDCI
f
iRAP
DAPI RAGE proSFTPC Merge
g
DAPI
RAGE
SFTPC
Merge
iRAP
D-iRAP
h
D-iRAP
DAPI RAGE SFTPC Merge
i
RAGE
SFTPC
proSFTPC
Signal intensity norm to DAPI
j
Cells %
Dead cells (DAPI+)
Live cells (DAPI-)
D0
D3
D12
D21

ED7

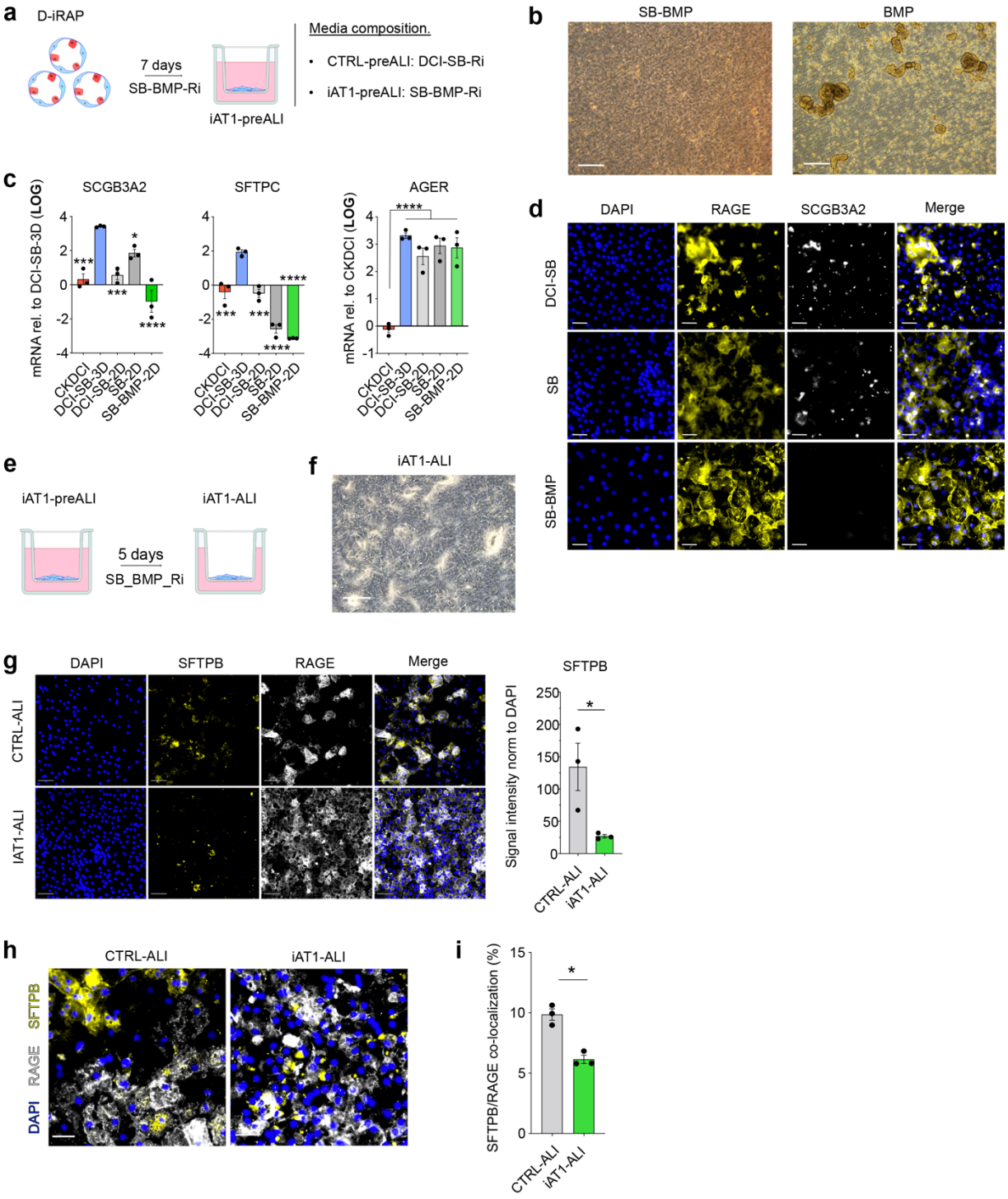
a
D-iRAP
7 days
SB-BMP-Ri
iAT1-preALI
Media composition.
• CTRL-preALI: DCI-SB-Ri
• iAT1-preALI: SB-BMP-Ri
b
SB-BMP
BMP
c
SCGB3A2
SFTPC
AGER
mRNA rel. to DCI-SB-3D (LOG)
mRNA rel. to CKDCI (LOG)
CKDCI
DCI-SB-3D
DCI-SB-2D
SB-2D
SB-BMP-2D
d
DAPI
RAGE
SCGB3A2
Merge
DCI-SB
SB
SB-BMP
e
iAT1-preALI
iAT1-ALI
5 days
SB_BMP_Ri
f
iAT1-ALI
g
DAPI
SFTPB
RAGE
Merge
CTRL-ALI
IAT1-ALI
SFTPB
Signal intensity norm to DAPI
CTRL-ALI
iAT1-ALI
h
CTRL-ALI
iAT1-ALI
SFTPB
RAGE
DAPI
i
SFTPB/RAGE co-localization (%)
CTRL-ALI
iAT1-ALI

ED8

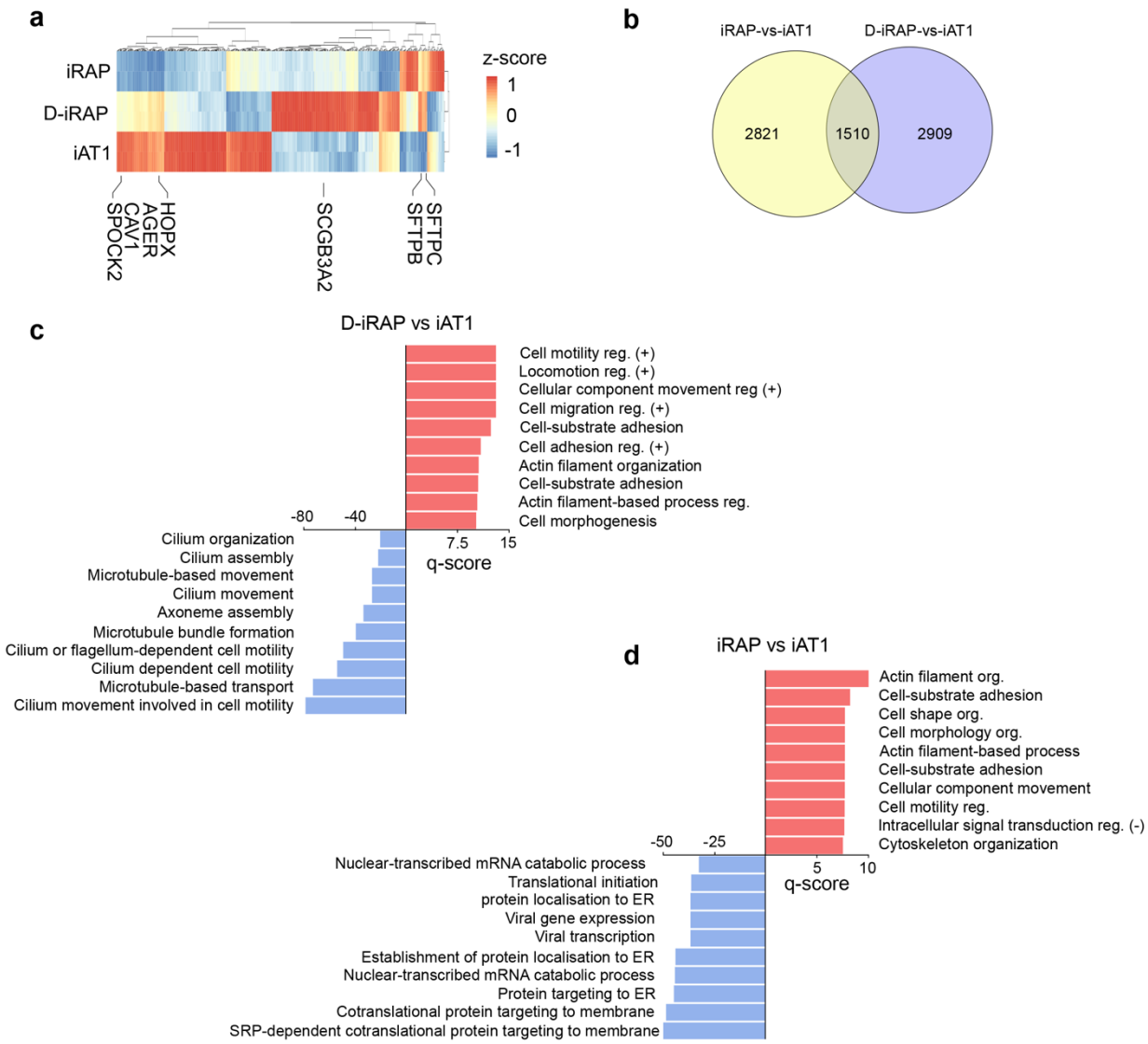
a
iRAP
D-iRAP
iAT1
z-score
1
0
-1
SPOCK2
CAV1
AGER
HOPX
SCGB3A2
SFTPB
SFTPC
b
iRAP-vs-iAT1
D-iRAP-vs-iAT1
2821
1510
2909
c
D-iRAP vs iAT1
Cell motility reg. (+)
Locomotion reg. (+)
Cellular component movement reg (+)
Cell migration reg. (+)
Cell-substrate adhesion
Cell adhesion reg. (+)
Actin filament organization
Cell-substrate adhesion
Actin filament-based process reg.
Cell morphogenesis
-80
-40
7.5
15
q-score
Cilium organization
Cilium assembly
Microtubule-based movement
Cilium movement
Axoneme assembly
Microtubule bundle formation
Cilium or flagellum-dependent cell motility
Cilium dependent cell motility
Microtubule-based transport
Cilium movement involved in cell motility
d
iRAP vs iAT1
Actin filament org.
Cell-substrate adhesion
Cell shape org.
Cell morphology org.
Actin filament-based process
Cell-substrate adhesion
Cellular component movement
Cell motility reg.
Intracellular signal transduction reg. (-)
Cytoskeleton organization
-50
-25
5
10
q-score
Nuclear-transcribed mRNA catabolic process
Translational initiation
protein localisation to ER
Viral gene expression
Viral transcription
Establishment of protein localisation to ER
Nuclear-transcribed mRNA catabolic process
Protein targeting to ER
Cotranslational protein targeting to membrane
SRP-dependent cotranslational protein targeting to membrane

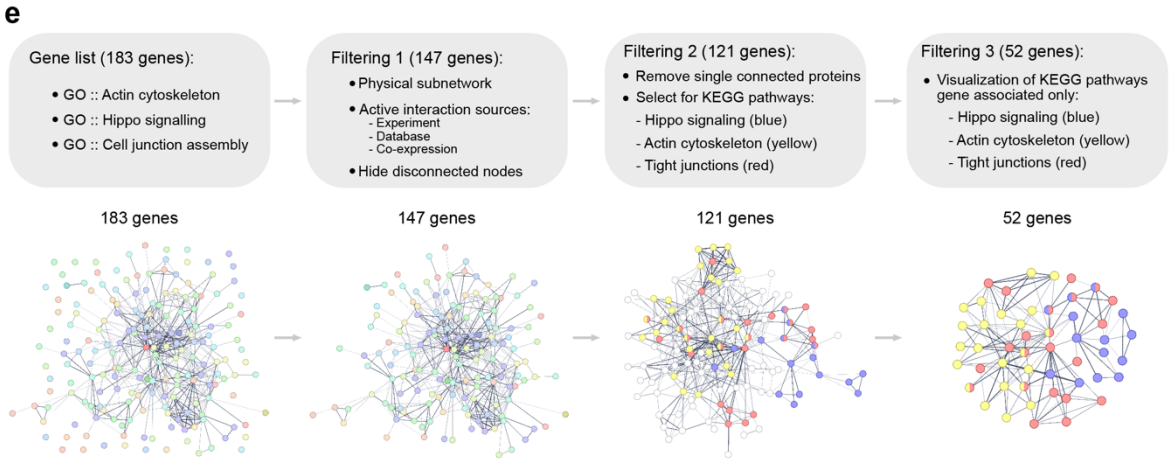
e
Gene list (183 genes):
• GO :: Actin cytoskeleton
• GO :: Hippo signalling
• GO :: Cell junction assembly
Filtering 1 (147 genes):
• Physical subnetwork
• Active interaction sources:
- Experiment
- Database
- Co-expression
• Hide disconnected nodes
Filtering 2 (121 genes):
• Remove single connected proteins
• Select for KEGG pathways:
- Hippo signaling (blue)
- Actin cytoskeleton (yellow)
- Tight junctions (red)
Filtering 3 (52 genes):
• Visualization of KEGG pathways gene associated only:
- Hippo signaling (blue)
- Actin cytoskeleton (yellow)
- Tight junctions (red)
183 genes
147 genes
121 genes
52 genes

ED9

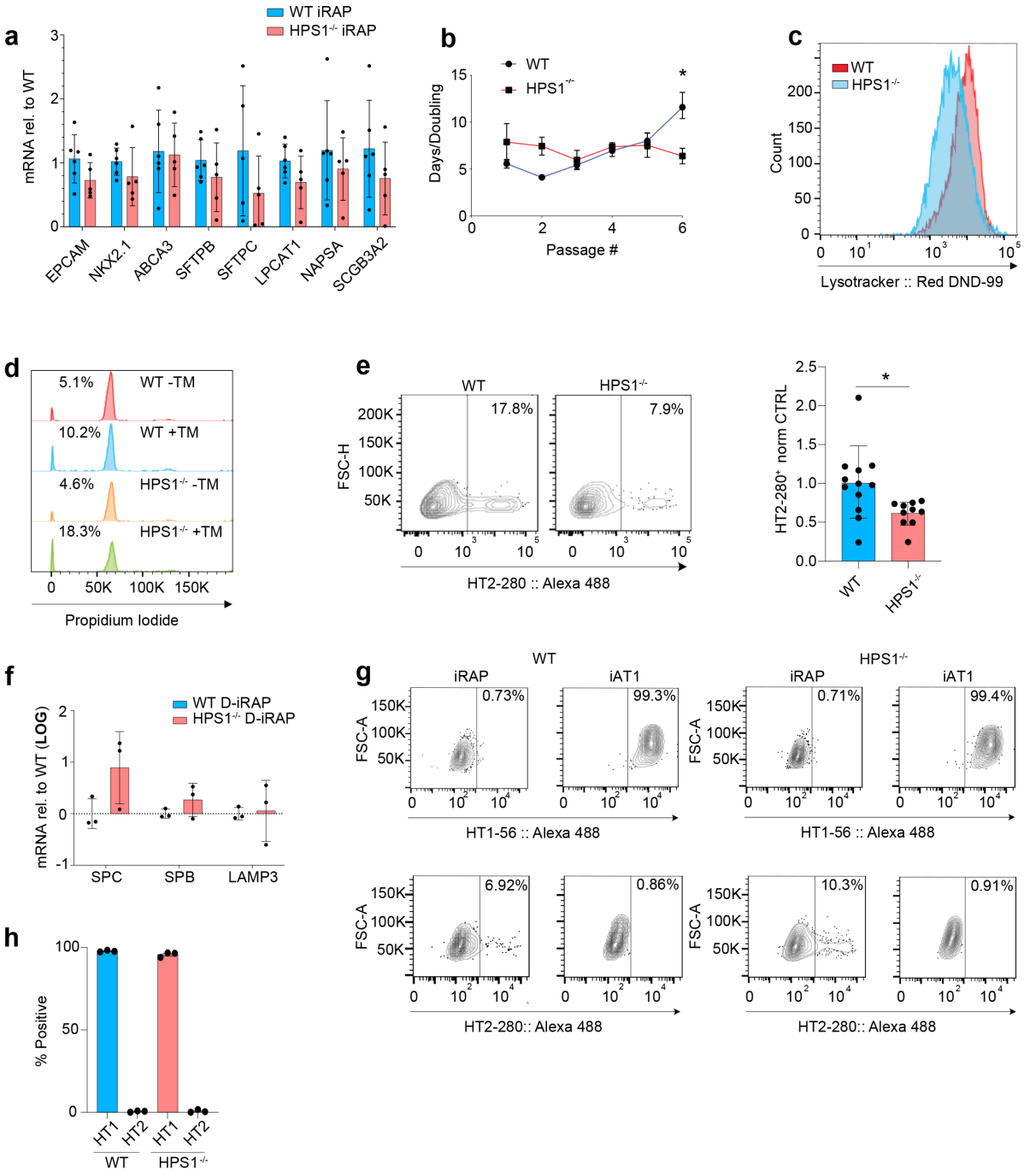
a
WT iRAP
HPS1-/- iRAP
mRNA rel. to WT
EPCAM
NKX2.1
ABCA3
SFTPB
SFTPC
LPCAT1
NAPSA
SCGB3A2
b
WT
HPS1-/-
Days/Doubling
Passage #
c
WT
HPS1-/-
Count
Lysotracker :: Red DND-99
d
5.1%
WT -TM
10.2%
WT +TM
4.6%
HPS1-/- -TM
18.3%
HPS1-/- +TM
Propidium Iodide
e
WT
HPS1-/-
17.8%
7.9%
FSC-H
HT2-280 :: Alexa 488
HT2-280+ norm CTRL
f
WT D-iRAP
HPS1-/- D-iRAP
mRNA rel. to WT (LOG)
SPC
SPB
LAMP3
g
WT
HPS1-/-
iRAP
iAT1
0.73%
99.3%
0.71%
99.4%
FSC-A
HT1-56 :: Alexa 488
6.92%
0.86%
10.3%
0.91%
HT2-280:: Alexa 488
h
% Positive
HT1
HT2
WT
HPS1-/-

Table S1: PCR primers

Gene	Forward primer	Reverse primer
ABCA3	CAGGCTGAGGGACAGGAG	TCCACAGAAGCCCTGAAGAT
AGER	GAGTCCGTGTCTACCAGATTC	ATCCAAGTGCCAGCTAAGAG
ASCL1	GAACTGATGCGCTGCAAACG	CGCAGTGTCTCCACCTTACT
BIP	TGTTCAACCAATTATCAGCAAACTC	TTCTGCTGTATCCTCTTCACCAGT
COL1A1	GGACACAGAGGTTTCAGTGGT	GCACCATCATTTCCACGAGC
COL3A1	GCAGGGTCTCCTGGTTCAAA	CGGGACCCATTTCGCCTTTA
EPCAM	CCATGTGCTGGTGTGTGAA	TGTGTTTTAGTTCAATGATGATCCA
FN1	AACAAACACTAATGTTAATTGCCCA	TCGGGAATCTTCTCTGTCAGC
GAPDH	AACTTTGGCATTGTGGAAGG	ACACATTGGGGGTAGGAACA
KRT17	CGGAGACAGAGAACCGCTAC	CTTGTACTGAGTCAGGTGGGC
KRT5	GGAATGCAGACTCAGTGGAGA	GCTGCTGGAGTAGTAGCTTCC
LAMP3	TGCTCATTTTTATGGGATTGC	TGAGTTTATTTGATGCCTTCATCTT
LPCAT1	GCCCTGTCTGTCGTCTGC	TCTTGCGCTCCGTACATCT
NAPSA	GTAGATGGAATCCTGAGCGAG	AGACAGAATGGGAAAACCGAG
NKX2.1	AGCACACGACTCCGTTCTC	GCCCACTTTCTTGTAGCTTTCC
P63	CTCGTCCACCAGTCCCTATAA	TGATGGAGAGAGAGCATCGAA
SCGB3A2	ACTCTGGGCATTTCTGTTGAG	CATCCACCTCCGCTCTTTATC
SFTPB	GAGCCGATGACCTATGCCAAG	AGCAGCTTCAAGGGGAGGA
SFTPC	GCAAAGAGGTCCTGATGGAG	ATCACCACGACGATGAGGA
SLC34A2	CACCATCTTGCTCATACTCTCC	GTCAACCATGCAAAGGGAAAG
SOX2	GCACATGAAGGAGCACCCGGATTA	CGGGCAGCGTGTACTTATCCTTCTT
sXBP1	CTGAGTCCGAATCAGGTGCAG	ATCCATGGGGAGATGTTCTGG
usXBP1	CAGCACTCAGACTACGTGCA	ATCCATGGGGAGATGTTCTGG

Table S2: Antibodies

Primary antibodies for immunofluorescence staining						
Name	**Host species**	**Clone number**	**Manufacturer and Catalog number**	**RRID**	**URL**	**Dilution Factor**
EPCAM	Goat	Polyclonal	R&D Systems Cat # : AF960	RRID:AB_355745	https://scicrunch.org/resolver/RRID:AB_355745	1:400
KI-67	Rabbit	D3B5	Cell Signaling Cat # : 9129S	RRID:AB_2687446	https://scicrunch.org/resolver/RRID:AB_2687446	1:200
NKX2.1	Rabbit	Polyclonal	Seven Hills Bioreagents Cat # : WRAB-1231	RRID:AB_2832953	https://scicrunch.org/resolver/RRID:AB_2832953	1:200
proSPC	Rabbit	Polyclonal	Millipore Sigma Cat # : AB3786	RRID:AB_91588	https://scicrunch.org/resolver/RRID:AB_91588	1:200

SCGB3A2	Rabbit	Monoclonal	Abcam Cat #:ab181853 (EPR11463)	-	-	1:250
SPB	Rabbit	Polyclonal	Seven Hills Bioreagents Cat # : WRAB-48604	-	-	1:500
AGER	Goat	Polyclonal	Bio-Techne R&D Cat# AF1145	RRID: AB_354628	https://www.antibodyregistry.org/AB_354628	1:200
Secondary antibodies for immunofluorescence staining						
Name	**Host species**	**Conjugate**	**Manufacturer and Catalog number**	**RRID**	**URL**	**Dilution Factor**
anti-Goat IgG (H+L)	Donkey	AF-488	Thermo Fisher Scientific; A32814	RRID:AB_2762838	https://scicrunch.org/resolver/RRID:AB_2762838	1:200
anti-Rabbit IgG (H+L)	Donkey	AF-488	Thermo Fisher Scientific; A21206	RRID:AB_2535792	https://scicrunch.org/resolver/RRID:AB_2535792	1:200
anti-mouse IgM Heavy Chain	Goat	AF-488	Thermo Fisher Scientific; A21042	RRID:AB_141357	https://scicrunch.org/resolver/RRID:AB_141357	1:200
anti-Goat IgG (H+L)	Donkey	AF-555	Thermo Fisher Scientific; A32816	RRID:AB_2762839	https://scicrunch.org/resolver/RRID:AB_2762839	1:200

anti-Rabbit IgG (H+L)	Donkey	AF-555	Thermo Fisher Scientific; A31572	RRID:AB_162543	https://scicrunch.org/resolver/RRID:AB_162543	1:200
anti-Goat IgG (H+L)	Donkey	AF-647	Thermo Fisher Scientific; A21447	RRID:AB_141844	https://scicrunch.org/resolver/RRID:AB_141844	1:200
Primary antibodies for Western blot						
Name	**Host species**	**Clone number**	**Manufacturer and Catalog number**	**RRID**	**URL**	**Dilution Factor**
GAPDH (HRP Conjugate)	Rabbit	14C10	Cell Signaling Technologies; 36835	-	-	1:5000
SFTPB	Rabbit	Polyclonal	Seven Hills Bioreagents Cat #: WRAB-48604	-	-	1:1000
SFTPC	Rabbit	Polyclonal	Seven Hills Bioreagents Cat #: WRAB-76694	-	-	1:1000
Secondary antibodies for Western blot						
Name	**Host species**	**Conjugate**	**Manufacturer and Catalog number**	**RRID**	**URL**	**Dilution Factor**

Anti-Rabbit IgG (H+L)	Goat	HRP	Cell Signaling Technologies; 7074	RRID:AB_2099233	https://scicrunch.org/resolver/RRID:AB_2099233	1:5000
Conjugated antibodies for flow cytometry						
Name	**Isotype**	**Conjugate**	**Manufacturer and Catalog number**	**RRID**	**URL**	**Dilution Factor**
anti-human CD326 (Ep-CAM)	Mouse IgG2b	APC	Biolegend Cat #: 324208	RRID: AB_756081	https://scicrunch.org/resolver/AB_756081	1:100
Primary antibodies for Flow Cytometry						
Name	**Host species**	**Clone Number**	**Manufacturer and Catalog number**	**RRID**	**URL**	**Dilution Factor**
HT2-280	Mouse	TB-27	Terrace Biotech Cat # : TB-27AHT2-280	RRID:AB_2832931	https://scicrunch.org/resolver/RRID:AB_2832931	1:100
HT1-56	Mouse	TB-29	Terrace Biotech Cat # : TB-29AHT1-56	RRID:AB_2847898	https://scicrunch.org/resolver/RRID:AB_2847898-2783354	1:100
Secondary antibodies for Flow Cytometry						

Name	Host species	Conjugate	Manufacturer and Catalog number	RRID	URL	Dilution Factor
anti-mouse IgM Heavy Chain	Goat	AF-488	Thermo Fisher Scientific; A21042	RRID:AB_141357	https://scicrunch.org/resolver/RRID:AB_141357	1:200
anti-mouse IgG (H+L)	Donkey	AF-488	Thermo Fisher Scientific; A-21202	RRID:AB_141607	https://scicrunch.org/resolver/AB_141607	1:200
anti-mouse IgM Heavy Chain	Goat	AF-594	Thermo Fisher Scientific; A-21044	RRID:AB_2535713	https://www.antibodyregistry.org/AB_2535713	1:200
Hashtag antibodies						
Name	**Host species**	**Clone Number**	**Manufacturer and Catalog number**	**RRID**	**URL**	**Dilution Factor**
TotalSeq™-B0251 anti-human Hashtag 1	Mouse	LNH-94; 2M2	BioLegend; 394631	RRID: AB_2814347	https://www.antibodyregistry.org/AB_2814347	1:400